

Université du Québec  
Institut National de la Recherche Scientifique  
Center for Energy Materials and Telecommunications

**Dynamics of semiconducting nanocrystals uptake into  
mesoporous TiO<sub>2</sub> thick films through electrophoretic deposition  
and its application in solar energy**

By  
**Lei Jin**

A thesis submitted to the Department of Energy, Materials and Communications in  
conformity with the requirements for the degree of Master of Philosophy

**Advisory Committee:**

President of the jury internal examiner	Mme Ana Tavares INRS-EMT, Université du Québec
External examiner	M. Richard Ares Université de Sherbrooke
Internal examiner	Mme Ana Tavares INRS-EMT, Université du Québec
Director of Research	M. Federico Rosei INRS-EMT, Université du Québec
Codirecteur de recherche	Mme Dongling Ma INRS-EMT, Université du Québec
	M. Alberto Vomiero Luleå University of Technology

## **ACKNOWLEDGEMENTS**

It is my great honor to spend one year and half to accomplish my graduate studies at Centre for Energy, Materials and Telecommunications, Institut National de la Recherche Scientifique (INRS-EMT), University of Quebec, Canada. Foremost, I would like to express my sincere gratitude to my supervisor, Prof. Federico Rosei, for continual guidance and support throughout the duration of my Master and research. Professionally, Dr. Rosei has supported me not only by providing systematic guidance and great effort in the scientific field, but also by offering me a chance to be a group coordinator to develop my social skills. And personally, he has always been a strong supporter and friend when I needed help. It is one of the most valuable experiences in my life being able to study under his supervision.

Besides my advisor, my sincere thanks also go to Prof. Alberto Vomiero, for his patience, motivation, enthusiasm, and immense knowledge. His guidance helped me in all the time of research and writing. I could not have imagined having a better development for my Master study without him.

I would also wish to give special thanks to the contributions to this work made by Dr. Haiguang Zhao, who made vital contributions and offered invaluable help and comments on my research.

I would like to acknowledge Prof. Dongling Ma, my co-supervisor at INRS-EMT, for her kind help and important comments on my project research. I am also grateful to all the group members from NFL (NanoFemtoLab) for their help throughout the work as well as other collaborators. Massive thanks to the departmental and technical staffs at INRS-EMT and all my friends who have made my research life so enjoyable.

Last but not least, I would like to give special thanks to my family: my parents Xiaoli Xing and Junli Jin, my sister Dong Jin, for their continuing love and heartily support. I also wish to express thanks to my Fiancé, Yang Liu, who loves me deeply and supports me selflessly. I thank my family and friends for supporting me spiritually throughout my life.

## ABSTRACT

Quantum dots (QDs), have been recognized as one type of the most promising photosensitizer for photoanode fabrication due to their unique and scalable optical properties where photoluminescence and absorption of the QDs are size-tunable. However, there are several major concerns with QD sensitized photoanodes: First, QDs should be deposited into mesoporous films effectively and without aggregation; Second, QDs have to be bound strongly onto mesoporous films; Last but not least, the charge transfer kinetics between QDs and wide-band-gap semiconductor has to be fast in order to achieve a highly efficient photoelectrode. The search for methods to achieve these requirements is attractive and challenging. Electrophoretic deposition (EPD), which is a straightforward technique for the uptake of nanoparticles into mesoporous films, has demonstrated highly effective in the preparation of high-efficiency QD-sensitized photoanodes. EPD consists in the application of an external potential between two electrodes immersed into a solution of the particles to be uploaded. Charged particles (both positive and negative) undergo a driving force that induces their penetration and grafting into the mesoporous photoanode. Unlike prior chemical linker-based methods, EPD does not require pretreatment of the  $\text{TiO}_2$ , and deposition time as short as 1 h is sufficient for effective coating. After EPD, the photoanode typically exhibits a high optical density, leading to complete absorption of solar radiation in the absorption range of the QDs. Despite the remarkable results obtained in terms of photoconversion efficiency (PCE), no systematic investigation is reported in literature on EPD of nanoparticles in mesoporous films so far. In the present thesis, we addressed this open issue and gave an exhaustive description of the phenomenon from the experimental point of view as well as from the point of view of the modeling of the physical chemical processes occurring during EPD. We investigated the uptake of colloidal QDs into  $\text{TiO}_2$  films using EPD. We examined  $\text{PbS}@\text{CdS}$  core@shell QDs, which are optically active in the NIR region of the solar spectrum and exhibit much increased long-term stability toward oxidation compared to their pure PbS counterpart, as demonstrated by X-ray photoelectron spectroscopy (XPS) and photoluminescence (PL). We applied Rutherford backscattering spectrometry (RBS) to obtain Pb depth profile into the  $\text{TiO}_2$  matrix. The

applied electric field induces the fast anchoring of QDs to oxide surface. Consequently, QD concentration in the solution contained in the mesoporous film drastically decreases, inducing a Fick-like diffusion of QDs. We modelled the entire process as a QD diffusion related to the formation of QD concentration gradient, and a depth-independent QD anchoring. EPD duration and applied voltages in the range 5 to 120 mins and 50 to 200 V were considered. Furthermore, we were able to determine the electric field-induced diffusion coefficient D for QDs and the characteristic time for QD grafting, in very good agreement with experiment. D increases from  $(1.5 \pm 0.4) \times 10^{-5} \mu\text{m}^2 \text{ s}^{-1}$  at 50 V to  $(1.1 \pm 0.3) \times 10^{-3} \mu\text{m}^2 \text{ s}^{-1}$  at 200 V. These results quantitatively describe the process of QD uptake during EPD, and can be used to tune the optical and optoelectronic properties of composite systems, which determine, for instance, the PCE of the photoanodes. The dynamics of EPD could also be applied to other different colloidal nanoparticles and quantum rod materials for sensitization of mesoporous films. In addition, we also demonstrated the increased stability of the core@shell structure compared to PbS QDs after EPD in terms of structure and optical properties. Based on our previous studies that confirmed a fast charge transfer from PbS@CdS to TiO<sub>2</sub>, PbS@CdS sensitized photoanodes can be strong candidates for the development of highly efficient and stable photoanodes in PV devices and photoelectrochemical (PEC) H<sub>2</sub> generation.

**KEYWORDS:** electrophoretic deposition, quantum dots, solar cells, quantum dot sensitized solar cell.

# TABLE OF CONTENTS

<b>ACKNOWLEDGEMENTS.....</b>	<b>II</b>
<b>ABSTRACT.....</b>	<b>III</b>
<b>TABLE OF CONTENTS.....</b>	<b>V</b>
<b>LIST OF TABLES .....</b>	<b>VII</b>
<b>LIST OF FIGURES.....</b>	<b>VII</b>
<b>LIST OF EQUATIONS .....</b>	<b>X</b>
<b>LIST OF ABREVATIONS.....</b>	<b>XI</b>
<b>1. INTRODUCTION .....</b>	<b>1</b>
1.1 QUANTUM DOTS (QDs) SENSITIZED PHOTOELECTRODES.....	1
1.1.1 <i>QDs work as light harvesters in solar cells (SCs)</i> .....	1
1.1.2 <i>QDs work as photosensitisers for H<sub>2</sub> production</i> .....	8
1.2 CHALLENGES IN QDs SENSITIZED PHOTOANODES .....	10
1.2.1 <i>Light harvesting</i> .....	10
1.2.2 <i>Uptake QD into mesoporous films</i> .....	11
1.2.3 <i>Stability</i> .....	12
1.3 THESIS OBJECTIVES AND CONTRIBUTIONS .....	13
1.4 THESIS ORGANIZATION .....	13
<b>2. EXPERIMENTAL.....</b>	<b>15</b>
2.1 MATERIALS.....	15
2.2 QDs AND TiO <sub>2</sub> FILMS PREPARATION .....	15
2.2.1 <i>Synthesis of PbS QDs</i> .....	15
2.2.2 <i>Synthesis of PbS@CdS QDs</i> .....	16
2.2.3 <i>Mesoporous TiO<sub>2</sub> films preparation</i> .....	17
2.2.4 <i>Uptake QDs into the mesoporous TiO<sub>2</sub> films thorugh EPD</i> .....	17
2.3 CHARACTERIZATIONS .....	18
2.3.1 <i>Scanning Electron Microscopy (SEM)</i> .....	18

2.3.2 <i>Transmission Electron Microscopy (TEM)</i> .....	19
2.3.3 <i>X-ray Photoelectron Spectroscopy (XPS)</i> .....	19
2.3.4 <i>Rutherford backscattering spectroscopy (RBS)</i> .....	20
2.3.5 <i>UV-visible (UV-vis) Spectroscopy</i> .....	22
2.3.6 <i>Photoluminescence (PL) Spectroscopy</i> .....	22
<b>3. DYNAMICS OF QD UPTAKE INTO MESOPOROUS TiO<sub>2</sub> THICK FILMS THROUGH EPD .....</b>	<b>23</b>
3.1 SYNTHESIS AND CHARACTERIZATION OF QDs IN SOLUTION AND IN TiO <sub>2</sub> FILMS .....	23
3.2 QD STABILITY AFTER EPD .....	26
3.3 DYNAMICS OF EPD .....	28
<b>4. PROMISING APPLICATIONS.....</b>	<b>37</b>
4.1 QDSCs FABRICATION .....	37
4.2 WATER SPLITTING .....	39
<b>5. CONCLUSION AND FUTURE PERSPECTIVES .....</b>	<b>41</b>
5.1 CONCLUSION .....	41
5.2 PERSPECTIVES .....	42
<b>6. REFERENCES .....</b>	<b>44</b>
<b>APPENDIX RESUME.....</b>	<b>57</b>

## LIST OF TABLES

Table 3.1 Dimensions and optical properties of pure and core@shell QDs investigated in this study. The overall size of PbS@CdS QDs is determined based on TEM observation, the core size is estimated from the position of the first excitonic peak and the shell thickness is estimated by simple subtraction. To identify the different samples, S M L labels are used according to their small, medium and large size, respectively.....	24
Table 3.2 PbS concentration and diffusion coefficient D as a function of the applied voltage in EPD.....	33

## LIST OF FIGURES

Figure 1.1 Image showing (a) colloidal PbS quantum dots. Inset: TEM image with resolution of 1.5 nm; (b) splitting of energy levels in QDs due to the quantum confinement effect, semiconductor band gap increases with decrease in size of the nanocrystals [22]; (c) solar spectrum [23] and corresponding tunable absorption spectra of QDs.....	3
Figure 1.2 Scheme (not to scale) of (a) QDSCs. Black arrows around the cell perimeter denote direction of electron flow (b) the energetics which drive electron and hole transport in a QDSCs. [25] .....	4
Figure 1.3 The equivalent circuit of a solar cell.[32].....	7
Figure 1.4 Getting the important parameters From the I-V Sweep. [34] .....	8
Figure 1.5 Band-edge positions of semiconductor photocatalysts relative to the energy levels of various redox couples in water. [40] .....	9
Figure 2.1 Image showing the air-free reaction setup for synthesizing PbS QDs. [90] .....	16
Figure 2.2 Cation exchange approaches for transferring PbS QDs into PbS@CdS. ·16	
Figure 2.3 (a) Illustration of the EPD system; (b) images of QDs/TiO <sub>2</sub> electrodes after 1 h of EPD, red and black labels corresponding to samples produced from positive and negative electrode of applied bias. .....	18
Figure 3.1 Size distributions of (a) PbS_M and (b) PbS@CdS_M QDs.....	23

Figure 3.2 Absorption spectra of (a) PbS and PbS@CdS QDs in solution. (b) Representative TEM image of PbS@CdS QDs. (c) EDX analysis of PbS@CdS QDs with ~3.0 nm core diameter (shell thickness ~0.2 nm) after anchoring to TiO <sub>2</sub> nanoparticles by using EPD for 30 min (negative TiO <sub>2</sub> electrode). Inset: SEM cross-section of a TiO <sub>2</sub> film. ....	24
Figure 3.3 Representative TEM images of PbS@CdS QDs loaded into TiO <sub>2</sub> at four different EPD durations (negative TiO <sub>2</sub> electrode): (a) 10 min (b) 30 min (c) 60 min (d) 120 min. Inset of (d): enlarged TEM image. The red circles highlight the presence of the QDs. (e) Dark field Scanning TEM image of TiO <sub>2</sub> nanoparticles covered by QDs. The high contrast between the TiO <sub>2</sub> and QDs allow precise identification of the position of the QDs on the surface of TiO <sub>2</sub> nanoparticles. ....	25
Figure 3.4 High resolution Pb 4f core level spectra Photoelectron spectra after correction of electrostatic charging obtained from (a) PbS_M quantum dot (b) PbS@CdS_M core@shell quantum dot on silicon (up) and upload into TiO <sub>2</sub> with EPD (down). ....	27
Figure 3.5 PL of (a) PbS_M QDs and (b) PbS@CdS_M QDs just after EPD and after 24 hours exposure to air. Benchmarking PL spectra of QDs in solution is also reported. ....	28
Figure 3.6 (a) RBS spectrum of TiO <sub>2</sub> mesoporous film sensitized with QDs for 120 minutes. The red curve is the RUMP code simulation. The surface edges for Ti, Cd and Pb are indicated by arrows. (b) RBS signal of the spectral region pertaining Pb signal for samples sensitized at different durations (5, 10, 30, 60, 120 minutes, from dark blue to light azure). A and B rectangles highlight the two different regions in which QD diffusion cannot be detected (A) or is clearly visible (B). ....	29
Figure 3.7 Pb atomic ration as a function of EPD time at the interface of TiO <sub>2</sub> /FTO for PbS@ CdS_L (red line) Black line corresponding to the change of the curvature. ....	30
Figure 3.8 Pb atomic ration as a function of EPD time at the surface of TiO <sub>2</sub> film of PbS@CdS_L ....	30
Figure 3.9 (a) Position of the parameter x <sub>0</sub> as a function of EPD time. Inset: illustration of the procedure to determine x <sub>0</sub> from a standard RBS spectrum. (b) Parameter x <sub>0</sub> versus square root of EPD time. (c) Experimental Pb yield (black line) versus film	

depth and simulated yield (red solid line) obtained from the diffusion coefficient D and the characteristic decay time  $\tau$  obtained from RBS data. The two different components contributing to the curve are reported: diffusion process of Pb from solution (red dotted line) and position-independent QD uptake (red dashed line). (d) Experimental (solid lines) and simulated (dashed lines) Pb yields for the complete series of EPD samples.

.....31

Figure 3.10 Pb distribution versus time and depth in  $\text{TiO}_2$  film under three different perspectives, based on the experimental parameters calculated for 200 V applied bias.

.....34

Figure 3.11(a)  $x_0$  versus square root of EPD time. (b) Diffusion coefficient D versus EPD voltage, and (c) Pb concentration versus depth at three different EPD voltages after 60 min EPD. Symbols: experiment; solid lines: simulations according to the values of D reported in Table 3.2 (d) Fraction of Pb introduced in the film by diffusion ( $\text{Pb}_{\text{Diff.}}$ ) at different voltages.  $\text{Pb}_{\text{Diff}}$  and the total Pb amount are calculated as the integral of Pb concentrations along film depth based on the two components illustrated in Figure 3.9 (c). .....35

Figure 4.1 Scheme of the QDSCs. ....38

Figure 4.2 J-V characteristics of QDSCs fabricated with  $\text{PbS}@\text{CdS}$  QDs-decorated  $\text{TiO}_2$  (device was coated with CdS and ZnS) under AM1.5G illumination with light intensity of  $100 \text{ mW/cm}^2$ . ....39

Figure 4.3 (a) Photocurrent density versus the applied voltage referenced to RHE and (b) photocurrent responses at 0.2 V vs RHE of  $\text{TiO}_2$ /colloidal QDs photoanode. ....41

## LIST OF EQUATIONS

<i>Equation 1.1</i> .....	2
<i>Equation 1.2</i> .....	5
<i>Equation 1.3</i> .....	5
<i>Equation 1.4</i> .....	5
<i>Equation 1.5</i> .....	5
<i>Equation 1.6</i> .....	5
<i>Equation 1.7</i> .....	6
<i>Equation 1.8</i> .....	6
<i>Equation 1.9</i> .....	6
<i>Equation 1.10</i> .....	6
<i>Equation 1.11</i> .....	8
<i>Equation 1.12</i> .....	8
<i>Equation 3.1</i> .....	31
<i>Equation 3.2</i> .....	32
<i>Equation 3.3</i> .....	33

## **LIST OF ABREVATIONS**

ATW.....	Atmospheric Thin Window
CB.....	Conduction band
CBD.....	Chemical Bath Deposition
CE.....	Counter electrode
DA.....	Direct Adsorption
DI.....	Deionized
DSSCs.....	dye-sensitized solar cells
EDX.....	Energy-dispersive X-ray spectroscopy
EIS.....	Electrochemical Impedance Spectroscopy
EL.....	Electrolyte
EPD.....	Electrophoretic deposition
FF.....	fill factor
FTO.....	Fluorine doped tin oxide
HRSEM.....	High Resolution Scanning Electron Microscope
I <sub>max</sub> .....	maximum current
I <sub>sc</sub> .....	short circuit current
MAA.....	Mercaptoacetic acid
NIR.....	Near Infrared
OA.....	Oleic Acid
ODE.....	Octadecene
OLA.....	Oleylamine
PCE.....	Photoconversion Efficiency
PEC.....	Photoelectrochemical

PL.....	Photoluminescence
PV.....	Photovoltaic
QDs.....	Quantum dots
QDSCs.....	Quantum dot-sensitized solar cells
QY.....	quantum yield
RBS.....	Rutherford backscattering spectrometry
redox.....	reduction-oxidation
SEM.....	Scanning Electron Microscopy
SILAR.....	Successive Ionic Layer Adsorption and Reaction
SCs.....	Solar Cells
TEM.....	Transmission Electron Microscopy
(TMS) <sub>2</sub> S.....	Bis (trimethylsilyl) sulfide
TOP.....	tri-octylphosphine
UV-vis.....	UV-visible
VB.....	valence bands
V <sub>max</sub> .....	maximum voltage
V <sub>oc</sub> .....	open circuit voltage
wbSC.....	wide-bandgap semiconductor
XPS.....	X-ray Photoelectron Spectroscopy

## **1. INTRODUCTION**

### **1.1 Quantum Dots (QDs) Sensitized Photoelectrodes**

Limiting the global temperature increase is one of the biggest challenges in the 21st century. [1] To limit increases in greenhouse gas ( $\text{CO}_2$ ) emissions, alternative energy sources to coal, oil and gas must be provided, such as power from wind and water, biomass, or solar energy. Compared to other clean sources, solar energy can provide our planet with about 10,000 times more energy than our global daily consumption. [2] In view of the intermittent nature of solar energy and our power consumption, the idea to convert light into electric power or chemical fuels is attracted raising awareness.

#### **1.1.1 QDs work as light harvesters in solar cells (SCs)**

It was not until 1839 that the photovoltaic (PV) effect was first discovered by French Physicist A. E. Becquerel, [3] essentially marking the dawn of human-based utilization of solar radiation. [4] A fundamental understanding of this phenomenon, given by Albert Einstein [5], paved the route for Bell Labs to develop a silicon PV cell [6] — the first solar cell capable of generating enough power from the sun to run electrical equipments every day. Solar panels based on this silicon p-n junction technology has attracted a lot of attention over the last few years and their commercially available efficiency has reached to 22%. [7] However, this class of PV devices suffers from problems of inherent limitations in silicon as a material, competing demand for high-grade silicon wafers, and high manufacturing costs. Herein further advancement in the research and development of new PV cells is required to increase the light to electric power conversion efficiencies and to reduce the price of solar panels.

The second generation PV devices consisting of polycrystalline semiconductor thin films, including amorphous silicon, Cu/In/Ga/Se (CIGS cells) and CdTe, which can bring down the price significantly, but their typical performance is 10 - 15% which needs to be enhanced for making them practically viable. [8, 9] In addition, the production of the second generation PV cells still requires vacuum processes and high temperature

treatments, resulting in a large consumption of energy associated with the scarce elements. Over the last few years, an intense worldwide effort was geared towards developing third generation PV cells by using wet chemistry synthetic routes for the preparation of suitably tailored nanomaterials. [10-19] Among the candidate sensitizers, QDs have attracted widespread attention, benefiting from its special optical properties. [20] Typically, a bulk semiconductor has continuous conduction and valence energy bands, separated by a fixed energy gap,  $E_g$ , which is the minimum energy required to excite an electron. The absorption of a photon with energy greater than the band gap energy could contribute to the excitation of an electron, leaving an orbital hole in the valence band to form an electron-hole pair (exciton), which has a finite size defined by the exciton Bohr radius (as shown in **Figure 1.1 (b)**). In bulk materials, the crystal lattice is much larger than the exciton Bohr radius, allowing free and independent movement of the exciton. However, in a QD, the size of the lattice is at or below the materials' exciton Bohr radius, translating the exciton to a confined volume less than what it naturally wants to occupy. This "confinement effect" results in particle-in-a-box like behavior, exhibiting as discrete energy levels (as opposed to a continuum of energy levels in a bulk sample, Figure 1.1 (b)). Specifically, the smaller the diameter of the QD is — the stronger the confinement is — the larger the bandgap of the QD is (Figure 1.1 (b)), as described in Equation 1.1 [21]:

$$E = E_g + (\hbar^2 \pi^2 / 2R^2) (1/m_e + 1/m_h) - 1.8e^2 / \epsilon R \quad \text{Equation 1.1}$$

where  $E_g$  is the band gap energy of the corresponding bulk material,  $\hbar$  is the Plank constant,  $m_e$  and  $m_h$  are the effective mass of electron and hole, respectively,  $e$  is the charge of the electron, and  $R$  and  $\epsilon$  are the radius and dielectric constant of QDs respectively. In other words, QDs with dimensions smaller than the exciton Bohr radius show size-dependent absorption. Therefore, if each single QD material can convert one region of the solar spectrum efficiently with the use of a single bandgap, then in theory, a high efficiency of light collection can be achieved by changing the bandgap of the material (Figure 1.1 (c)), which means by changing only the composition and nanoparticles' size of QDs. Benefiting from the ability to tune the optical properties of

QDs by manipulating their sizes and compositions, QDs were introduced into third generation solar cells as sensitizers.

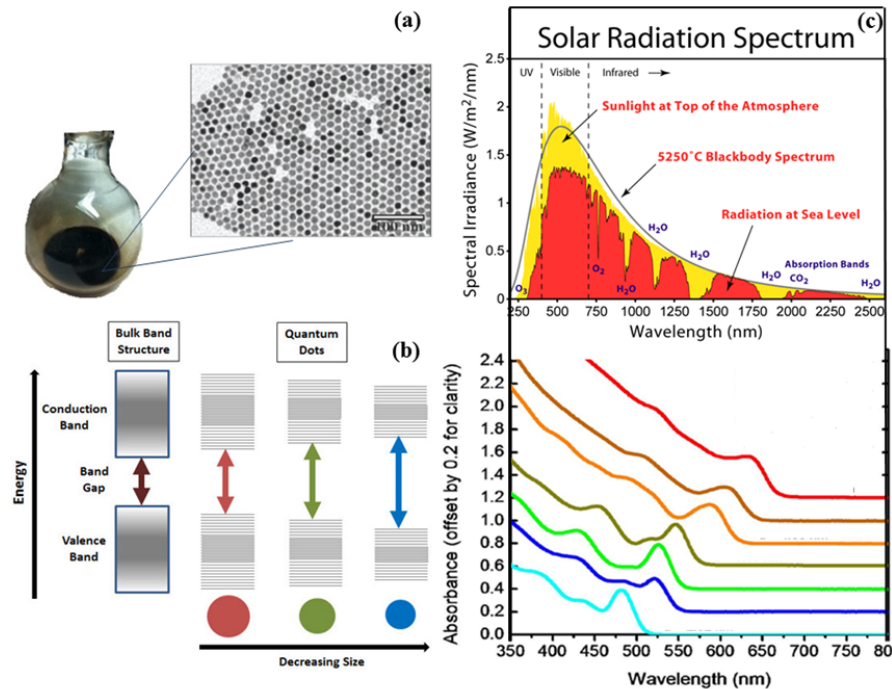


**Figure 1.1** Image showing (a) colloidal PbS quantum dots. Inset: TEM image with resolution of 1.5 nm; (b) splitting of energy levels in QDs due to the quantum confinement effect, semiconductor band gap increases with decrease in size of the nanocrystals [22]; (c) solar spectrum [23] and corresponding tunable absorption spectra of QDs.

#### 1.1.1.1 Construction of quantum dot-sensitized solar cells (QDSCs)

As a cost-effective alternative to silicon-based PV cells, QDSCs can be regarded as a derivative of dye-sensitized solar cells (DSSCs) which was first reported by O'Regan and Grätzel in 1991. [24] Nanostructured wide-bandgap semiconductor (wbSC), such as TiO<sub>2</sub> (3.2 eV), which forms into a highly porous nanocrystalline, had been selected as the sensitizer scaffold, due to their high surface to volume ratio (their real surface area is larger than their geometric area). **Figure 1.2** (a) shows a scheme of the basic design of a QDSC. The QD-sensitized nanostructures are immersed into the reduction-oxidation (redox) electrolyte, and the circuit is closed by a counter electrode (CE). The QDs, which graft to the surface of wbSCs, absorb light and create an exciton. Then the exciton dissociation occurs at the QD/wbSC interface, and the resulting electron is

injected from excited levels of QD into the conduction band (CB) of the wbSC. A liquid electrolyte completes the electrochemical system and allows QD neutralization after electron injection.

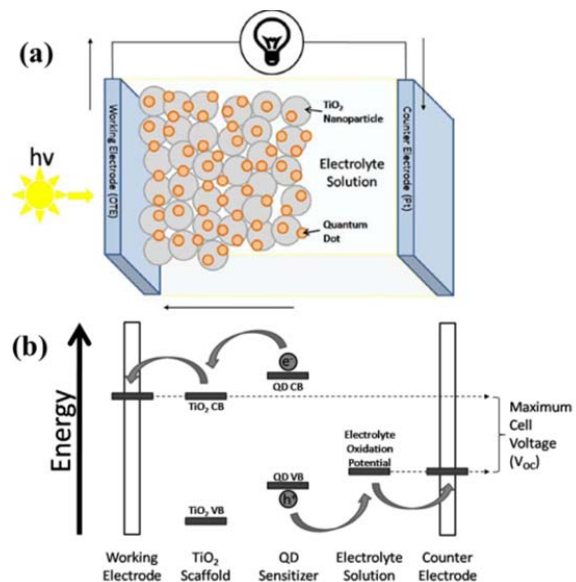


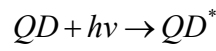
**Figure 1.2** Scheme (not to scale) of (a) QDSCs. Black arrows around the cell perimeter denote direction of electron flow (b) the energetics which drive electron and hole transport in a QDSCs. [25]

### 1.1.1.2 Electron Transfer Reactions within QDSCs

To understand the effect of energetics on solar cell, an energy diagram was shown in Figure 1.2 (b)), with a direct view on the energetics of the working electrode, QDs sensitizer, the TiO<sub>2</sub> scaffold film, the electrolyte as well as the counter electrode. When the CB and valence bands (VB) of QDs and TiO<sub>2</sub> match suitably, the electrons and holes can accumulate in two separate particles, allowing high possibilities to be captured at the surface of working electrode. In order for the reactions to take place, the CB of QDs must lie above the CB of TiO<sub>2</sub>, and redox potential of the electrolyte must lie between valence band of QDs and conduction band of TiO<sub>2</sub>. Then once the QDs are excited, electrons and holes can be energetically drawn to transfer to lower energy states (more negative in vacuum scale) and higher energy states (more positive in vacuum scale) respectively.

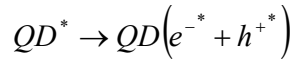
If we consider the reactions in an ideal manner: the electron travels from the QDs, through the external circuit, the electrolyte, and back to the QDs; in parallel, the hole travels in the opposite direction, then the reactions contributing to the ideal device performance can be figured out as below:

- a) QD is excited by absorbing a photon with energy higher than its bandgap, converting solar energy present in an electromagnetic wave to the potential energy difference between an electron and a hole:



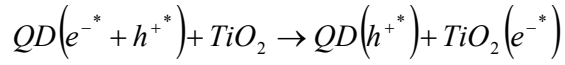
*Equation 1.2*

- b) An electron-hole pair in the form of an exciton, or an electrostatically bound pair is formed after the absorption event immediately. If the characteristic exciton binding energy of materials is less than the available thermal energy present in the system, the exciton can dissociate into free carriers: [26, 27]



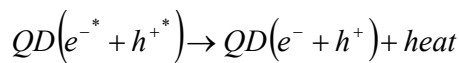
*Equation 1.3*

- c) The electron can be transferred from a thermally excited state within the QD to the CB of TiO<sub>2</sub>, a process known as hot electron injection: [28, 29]



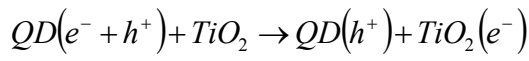
*Equation 1.4*

In the absence of this reaction above, thermally excited electrons (holes), can transfer a portion of their potential energy to heat and then energetically move from the quasi-continuum of states, which are above (below) the CB (VB) band edge, to their lowest energy configuration at the CB (VB) band edge: [30, 31]



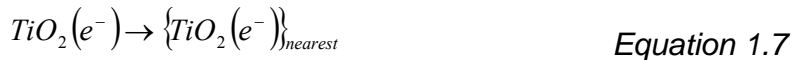
*Equation 1.5*

The photogenerated electron can be transferred from the QD to TiO<sub>2</sub>, resulting in spatial charge separation:



*Equation 1.6*

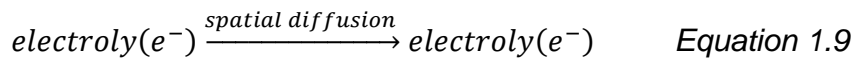
- d) The mesoporous morphology of  $TiO_2$  provides a high surface area for QDs uptake, so that the photogenerated electrons injected into its neighboring  $TiO_2$  should transport through other  $TiO_2$  particles before being collected at the working electrode:



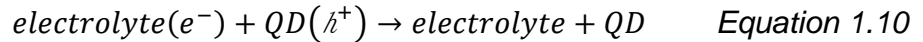
- e) During the migration to the working electrode, the electrons can also have possibility to be transferred to the electrolyte molecules which are in contact with the  $TiO_2$ , reducing the electrolyte:



- f) The reduced electrolyte should spatially diffuse through the liquid portion of the device:



- g) When a QD with a photogenerated hole comes across with the reduced electrolyte, the electrical circuit is closed, accompanied by the regeneration of the QDs:



#### **1.1.1.3 The I-V characteristics of QDSSCs**

PV cells are devices that absorb photons from a light source and release electrons, causing an electric current to flow once the cell is connected to a load. To understand the electronic behavior of a solar cell, an electrically equivalent model based on discrete electrical components can be established, as shown in **Figure 1.3**. It is evident that the current produced by the solar cell is equal to that produced by the current source, minus that which flows through the diode, minus that which flows through the shunt resistor.

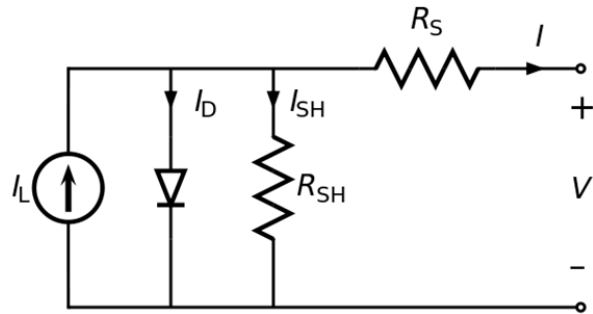


**Figure 1.3** The equivalent circuit of a solar cell. [32]

To characterize solar cells, the most obvious and important measures is the total amount of electrical power produced for a given amount of solar power shining on the cell, which is known as the photoconversion efficiency (PCE). Electrical power is the product of current and voltage, so the maximum values for these measurements are important. In theory, the maximum voltage ( $V_{oc}$ ) generated by QDSCs is simply the difference between the (quasi-) Fermi level of the QD sensitized  $TiO_2$  and the redox potential of the electrolyte. Although the QDs can convert absorbed photons into free electrons in the  $TiO_2$ , only photons with energy higher than the bandgap of QD ultimately produce current. The rate of photon absorption depends upon the absorption spectrum of the sensitized  $TiO_2$  layer and upon the solar flux spectrum. The overlap between these two spectra determines the maximum possible photocurrent ( $I_{sc}$ ). To determine the maximum power from a QDSCs, a parameter which in conjunction with  $V_{oc}$  and  $I_{sc}$ , was defined as "fill factor" (FF). These important parameters about the cell's performance, including its maximum current ( $I_{max}$ ) and voltage ( $V_{max}$ ), open circuit voltage ( $V_{oc}$ ), short circuit current ( $I_{sc}$ ), FF and its PCE (by dividing a cell's power output (in watts) at its maximum power point ( $P_m$ ) by the input light ( $E$ , in  $W/m^2$ ) and the surface area of the solar cell ( $A_c$  in  $m^2$ )), are derived from the current-voltage (I-V) characterization of a solar cell, which is the superposition of the IV curve of the solar cell diode in the dark with the light-generated current, [33] as shown in **Figure 1.4**.

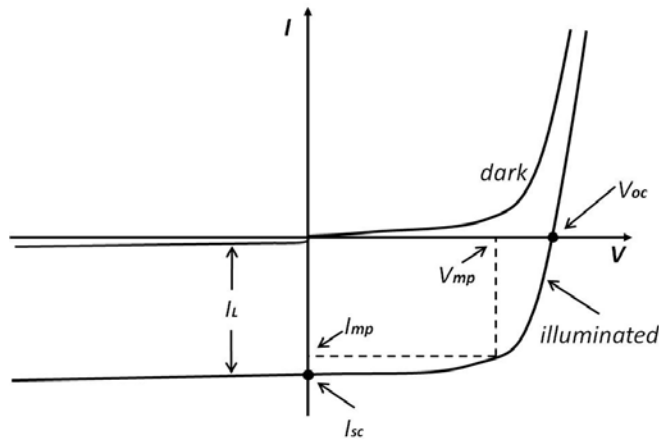


**Figure 1.4 Getting the important parameters From the I-V Sweep.[34]**

Regarding the solar cell as an ideal diode under illumination, the relationship between dark saturation current and  $V_{oc}$  can be inferred from the equation:

$$J = J_0 \left[ \exp \left( \frac{qV}{nkT} - 1 \right) \right] - J_{sc} \quad \text{Equation 1.11}$$

where  $J_0$  is the dark saturation current density ( $\text{A/cm}^2$ ),  $J_{sc}$  is the short circuit current density ( $\text{A/cm}^2$ ), and  $n$  is the ideality factor. Assuming that the  $J_{sc}$  is voltage independent and  $J_{sc} \gg J_0$ , the  $V_{oc}$  is then given by setting  $J$  to 0:

$$V_{oc} = \frac{n k T}{q V} \ln \left( \frac{J_{sc}}{J_0} \right) \quad \text{Equation 1.12}$$

From equation Eauation 1.12,  $V_{oc}$  is proportion to  $\ln \left( \frac{J_{sc}}{J_0} \right)$ , and therefore  $J_0$  needs to be as small as possible to maximize  $V_{oc}$ .

### 1.1.2 QDs work as photosensitisers for H<sub>2</sub> production

In view of the intermittent nature, convenient transportation and night-time use of solar energy, the search for method to convert solar energy into a storable form is attractive and challenging. [35, 36] Photoelectrochemical (PEC) solar driven hydrogen production with semiconductor materials [37] appears to be a much more attractive route because the use of H<sub>2</sub> chemical bonds to store solar energy combines the advantages of high energy storage densities, ease of transportation, cost-effective and

having clean water as the only by-product. [38, 39] Generally, PEC cell presents redox reactions driven by electron-hole pair created by incident photons, namely, the holes oxidize water/hole scavenger at the surface of the photoanode, and the electrons migrate to the counter electrode to reduce water and produce hydrogen. Herein, what is needed and challenging is the development of inexpensive semiconducting materials with suitable conduction and valence band energies, which have not only strong sunlight absorption and effective charge separation, but also high photochemical stability.

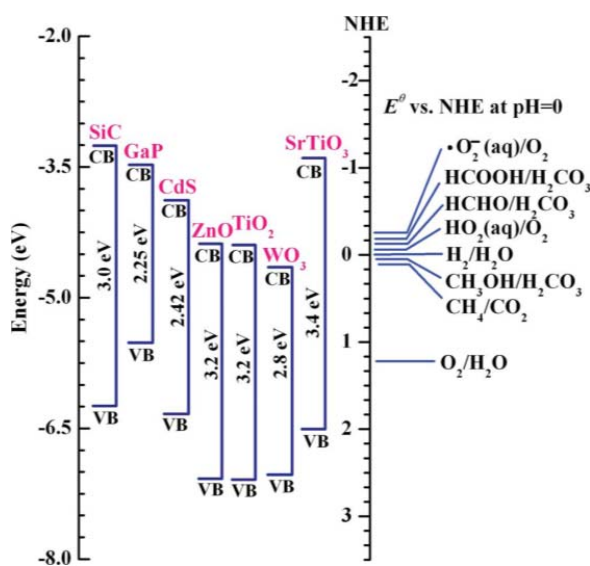


**Figure 1.5 Band-edge positions of semiconductor photocatalysts relative to the energy levels of various redox couples in water. [40]**

Since the Honda-Fujishima effect of water splitting using a  $\text{TiO}_2$  electrode was reported in the early 1970s [38], extensive efforts have been made to construct an efficient PEC water-splitting system and to develop new semiconductor materials for efficient photoelectrodes. The aim of PEC material fabrication is to design a photoelectrode that has the potential to satisfy most of the requirements [41]: (a) sufficient visible light absorption (i.e. band gap) in the range of 1.5 to 2.0 eV; (b) efficient separation of photo-generated electron-hole pairs and fast transport of electrons and holes to prevent their recombination; (c) favourable alignment of conduction and valence band edge position with respect to redox potential of water and the resultant photovoltage output to drive the reaction; (d) non-corrosive and high chemical stability in

the electrolyte; and (e) low cost. **Figure 1.5** lists bandgap, energy levels of the current photoelectrode materials that researchers focused on. Upon examining several typical semiconductors for PEC applications, the choice of available materials with band gaps ranging between 1.5 and 2.0 eV is limited and thus new semiconductors with narrow bandgap and novel configurations for photoelectrode are needed for practical applications.

Numerous studies have reported large band gap semiconducting oxides such as TiO<sub>2</sub> can be developed for H<sub>2</sub> evolution with long-time stability in aqueous electrolyte [42]. However, PEC utility of TiO<sub>2</sub> is limited by its UV-responsive band gap of approximately 3.2 eV. Therefore much effort has been made in the attempt to prepare TiO<sub>2</sub>-based photocatalysts that can efficiently improve light absorption in a broader spectral region. Such efforts include doping TiO<sub>2</sub> with metal/nonmetal ions to induce a red shift to the band gap, [43, 44, 45] and coupling TiO<sub>2</sub> with lower-band-gap semiconductors. [63, 46] Among the low-band-gap semiconductors, the QD is an attractive semiconductor as their band gap is dependent on their size (Figure 1.1 (b,c)) and the existing technology can produce QDs optically active in the visible and near infrared (NIR) spectral region.

## 1.2 Challenges in QDs sensitized photoanodes

### 1.2.1 Light harvesting

An intense effort to boost the development of PV architectures [10-13] and PEC photoanode [47-50] lies on application of chalcogenide QDs, including CdS, CdSe and CdTe as light harvesters to sensitize TiO<sub>2</sub>, forming a convenient heterostructured platform. However, these QDs are optically active in the visible range. Effectively, photons with energies lower than the bandgap do not get absorbed, in other words, QDs are optically active in the visible region largely ignores NIR light and wastes about 40 percent of the solar energy reaching Earth's surface, reducing output. Herein, QDs that are optically active in the NIR spectral region, such as PbS [51] and PbSe [52] have attracted enormous interest as sensitizers in recent years, while the investigations are still limited so far.

### 1.2.2 Uptake QD into mesoporous films

In a particular configuration of QD sensitized photoanode, [53] the QDs are grafted on the surface of a wide band gap semiconductor, [54, 55] absorbing light and creating an exciton. Then exciton dissociation occurs at the QD/oxide interface, and then the electron is injected into the oxide that acts as electron transporter. [56] For this reason, one of the important challenges is to apply a low-cost process to incorporate QDs onto the oxide and to achieve effective QD-electrode junctions that would promote charge separation, while minimizing surface charge trapping and charge losses.

*In situ* growth methods have been widely used to prepare QD-decorated TiO<sub>2</sub> photoanodes, including chemical bath deposition (CBD), [57, 58] and successive ionic layer adsorption and reaction (SILAR). [59, 60] Although a direct contact between the oxide and the QDs is achieved in this way, there is no independent control of QD coverage and size. [13] These drawbacks can be avoided if QDs are synthesized in form of colloids before sensitization of the oxide, and then grafted onto the oxide surface. Typically, three main different techniques are used for preparation of colloidal QD-decorated oxide thick films: linker-assisted adsorption, [58, 61] direct adsorption (DA), [62] and electrophoretic deposition (EPD). [63] In most cases, the attachment of the QDs to the mesoporous electrode is achieved by using a molecular linker between QD and the oxide particle, and one to several days are needed to achieve the desired coverage and photoanode optical density for QDs with hydrophobic ligand. [64] In case of hydrophilic ligands, QD uptake is typically much faster (several hours), [65] but the linker molecule may act as a barrier for electron injection, affecting the photovoltaic properties. [66] DA method is based on solvent/non-solvent precipitation of QDs from the solution into the mesoporous film: the tendency of the QDs to agglomerate in solution may lead to uneven and polydisperse surface coverage. [67] EPD, a widely used technique, is based on the motion and grafting of charged particles under an applied electric field, and presents several advantages over the other methodologies, such as the low cost, short duration of the process,

simple equipment, homogeneous surface coverage and formation of a uniform QD layer of controlled thickness. [68, 69]

EPD was previously employed to deposit semiconducting, [70, 71] metallic, [72, 73] and insulating [74, 75] nanoparticles on conductive substrates or polymers film. [73, 76] The first application of EPD for solar cells was reported for the deposition of TiO<sub>2</sub> nanoparticles. [74] Colloidal CdSe QDs were deposited via EPD on a flat thin film as a proof of concept for PV applications, yielding low PCEs ( $\sim 10^{-6}\%$ ) due to the very low optical density of the solar cell. [77] In order to increase the active area, CdSe QDs were incorporated into porous TiO<sub>2</sub> layers several microns thick, [63] reaching efficiencies as high as 1.7%, under 1 sun illumination. Mora-Seró and co-workers [78] have prepared QDs sensitized photoanodes by depositing the colloidal PbS and PbSeS QDs into TiO<sub>2</sub> mesoporous film via EPD. A strong relationship between QD sizes, EPD time and device performance was observed, clearly identifying the factors in EPD that are essential for the successful development of QDs sensitized photoanodes. In addition, the decrease of recombination resistance with EPD time unambiguously demonstrated that conformal coverage of TiO<sub>2</sub> surface would reduce charge recombination from TiO<sub>2</sub> to electrolyte. [79] For these reasons, suitable control of the parameters determining QD uptake and oxide coverage is mandatory. However, so far, only generic demonstration of almost constant QD penetration into films is claimed, based on low-resolution X-ray spectroscopy (EDX) analysis, [77] and no systematic investigation of QD uptake is found in literature.

### 1.2.3 Stability

One of the biggest challenges for both PV devices and PEC H<sub>2</sub> production is the development of a long-term stable photoanode. In fact, QDs, owing to their large surface-to-volume ratio, are very sensitive to surface defects and oxidation, which cause charge trapping, [80] leading to decrease of PCE. [81] For this reason, QDs are typically capped with organic surface ligands, [82, 83] while the dangling bonds remaining on the QD surface can act as carrier trapping sites if partial ligand unpassivation occurs. [84] Recent studies [85, 86, 87] have revealed that a robust, larger band gap inorganic shell can provide more complete passivation for the QD surface,

contributing to largely improved chemical, thermal, photochemical stability, and acceptable charge injection rate in QDs with suitable core size and shell thickness. [88]

### 1.3 Thesis objectives and contributions

To address all these challenges and issues, I investigated more deeply on QDs sensitized photoanodes by coupling high-quality PbS or PbS@CdS quantum dots into TiO<sub>2</sub> thick mesoporous films. The objectives of the projects are the following:

- 1) Synthesize high-quality PbS and PbS@CdS core@ shell QDs, characterize their structure and properties.
- 2) Uptake of *ex-situ* PbS or PbS@CdS QDs into TiO<sub>2</sub> mesoporous thick films using EPD and investigation the distribution and stability of QD after EPD.
- 3) A systematic investigation of the dynamics of NIR QDs loaded into TiO<sub>2</sub> mesoporous film via EPD.
- 4) Investigation of the influence of EPD time and voltage on the QD uptake process by using PbS@CdS core@shell QDs as highly stable light harvesters.
- 5) Applied the EPD dynamic to prepare QD sensitized photoanodes with suitable control over QD uptake and oxide coverage, for PV devices fabrication and PEC H<sub>2</sub> production.

### 1.4 Thesis Organization

This thesis is divided into five parts and organized as follows:

**Chapter 1** introduces the topic of this thesis and outlines the motivation for this work.

**Chapter 2** describes the experimental details of the synthesis for PbS and PbS@CdS QDs preparation and the main experimental characterization methods used throughout this works.

**Chapter 3** illustrates the dynamics of QD into TiO<sub>2</sub> photoanodes as obtained from Rutherford backscattering spectrometry.

Related publication:

1. L. Jin, H. Zhao, D. Ma, A. Vomiero, and F. Rosei. Dynamics of semiconducting nanocrystal uptake into mesoporous TiO<sub>2</sub> thick films by electrophoretic deposition. *Journal of Materials Chemistry A*, 3, 847 (2015).
2. H. Zhao, Z. Fan, H. Liang, G. S. Selopal, B. A. Gonfa, L. Jin, A. Soudi, D. Cui, F. Enrichi, M. M. Natile, I. Concina, D. Ma, A. O. Govorov, F. Rosei, and A. Vomiero. Controlling photoinduced electron transfer from PbS@CdS core@shell quantum dots to metal oxide nanostructured thin films. *Nanoscale*, 6, 7004 (2014).

**Chapter 4** states the promising applications of PbS@CdS sensitized photoanodes in the field of solar energy conversion.

**Chapter 5** briefly summarizes the most important contributions of this work and presents the prospect to optimize the applications in solar energy conversion.

## **2. EXPERIMENTAL**

In this chapter, I introduce the synthesis details for colloidal PbS and PbS@CdS QDs related to the results to be presented and discussed in Chapter 3. Firstly, PbS QDs were synthesized with hot injection method by using oleic acid as ligands. Then I turned to synthesize PbS@CdS QDs, via cation exchange in the organic phase, which show largely enhanced quantum yield (QY) of PbS core QDs. After that, I focused on the uptake of high-quality PbS and PbS@CdS QDs on TiO<sub>2</sub> by EPD.

### **2.1 Materials**

Lead chloride (98%), sulfur (100%), oleylamine (OLA) lead acetate trihydrate, trioctylphosphine (TOP 90%), bis (trimethylsilyl) sulfide (TMS)<sub>2</sub>S, (technical grade, 70%), cadmium oxide (99%), oleic acid (OA), mercaptoacetic acid (MAA), 1-octadecene (ODE), acetonitrile, and hydrochloric acid were obtained from Sigma-Aldrich Inc. Hexane, toluene, and ethanol were purchased from Fisher Scientific Company. Titania paste with nanoparticles of different sizes (18NR-AO, a blend of active anatase particles ~20 nm and larger anatase scatter particles up to 450 nm) and a 20 nm particle size paste (18NR-T) were supplied by Dyesol (Queanbeyan, Australia). All chemicals were used as purchased.

### **2.2 QDs and TiO<sub>2</sub> films preparation**

#### **2.2.1 Synthesis of PbS QDs**

PbS QDs with diameter of ~3.0 nm were synthesized with hot injection method by using OA as ligands (reaction setup can be seen in **Figure 2.1**). [89]

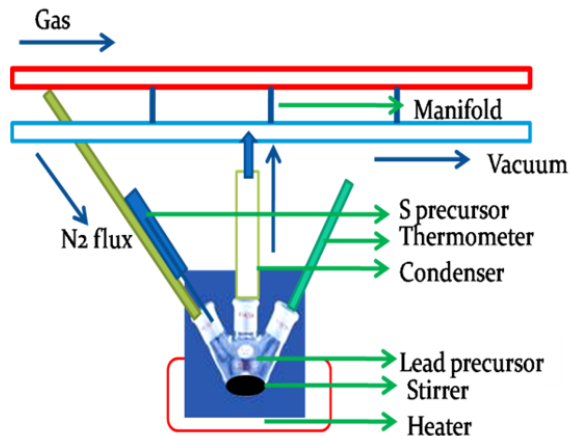


**Figure 2.1** Image showing the air-free reaction setup for synthesizing PbS QDs. [90]

- 1) Typically, a mixture of lead acetate trihydrate (1 mmol), OA (1.2 mL), TOP (1 mL), and ODE (15 mL) were heated to 150 °C for 1 h;
- 2) Then, the system was cooled down to ~100 °C under vacuum for 15 min;
- 3) Subsequently, a sulphur precursor solution was prepared by mixing (TMS)<sub>2</sub>S (0.5 mmol) with 0.2 mL of TOP and 4.8 mL of the mixture was quickly injected into the reaction flask at 130 °C;
- 4) Then, the reaction was quenched by cold water.

PbS QDs were precipitated with ethanol, centrifuged to remove unreacted lead oleate and free OA molecules and then re-dispersed in toluene.

### 2.2.2 Synthesis of PbS@CdS QDs

PbS@CdS QDs were synthesized via a cation exchange method, [87] as illustrated in **Figure 2.2**.

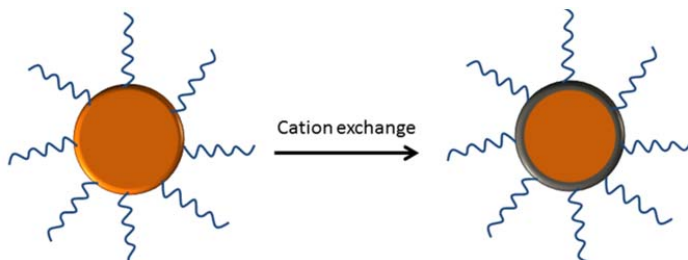


**Figure 2.2** Cation exchange approaches for transferring PbS QDs into PbS@CdS.

- 1) Typically, CdO (2.3 mmol), OA (2 mL) and ODE (10 mL) were heated to 255 °C under N<sub>2</sub> for 20 min.
- 2) The clear solution was cooled down to 155 °C under vacuum for 15 min.
- 3) The flask was then reopened and the N<sub>2</sub> flux was restored.
- 4) PbS QDs suspension in toluene (1 mL, Absorbance = 3 at the first exciton peak) was diluted in 10 mL toluene, bubbled with N<sub>2</sub> for 30 min and then heated to 100 °C immediately.
- 5) The Cd/OA mixture was added via a syringe.
- 6) The solution was maintained at 100 °C for 1-30 minutes and then cooled down to room temperature with cold water.

PbS@CdS QDs with tunable core sizes and shell thickness in the range 0.2 - 0.5 nm were synthesized by choosing different starting PbS sizes together with different reaction parameters (Pb-to-Cd ratio and reaction time).

### **2.2.3 Mesoporous TiO<sub>2</sub> films preparation**

Fluorine doped tin oxide (FTO) coated glass substrates (Pilkington, bought from Hartford Glass Co. Inc., USA) with sheet resistance 15 Ω/square were cleaned with ethanol, thoroughly rinsed with deionized (DI) water and dried in a N<sub>2</sub> stream. Then the titania paste was deposited on the top of FTO by tape casting and dried in air for 10 mins. The photoanodes were then fired on hot plate at 80 °C for 60 mins and subsequently sintered at 450 °C for 30 mins, forming a transparent film with thickness ~6 μm measured using a stylus profilometer.

### **2.2.4 Uptake QDs into the mesoporous TiO<sub>2</sub> films through EPD**

The EPD system is presented in **Figure 2.3** and the experimental details are described below:

- 1) QDs were dispersed in toluene, with a pair of TiO<sub>2</sub>/FTO slides vertically immersed in the QDs solution and facing to each other (Figure 2.3 (a)). The distance between

them was adjusted at 1 cm and the deposition area of the electrodes was about 0.72 cm<sup>2</sup>.

- 2) A constant voltage of was applied for a certain time. To investigate the EPD dynamic, applied voltages and duration in the range 50 to 200 V and 5 to 120 mins were considered respectively.
- 3) After EPD of QDs, both the positive and negative TiO<sub>2</sub> electrodes were colored (Figure 2.3 (b)), consistently with previous studies, [63, 78] indicating the deposition of negatively and positively charged QDs in terms of the preferential removal of the passivating ligand molecules. To wash off unbounded QDs after the EPD process, the samples were rinsed several times with toluene and dried with N<sub>2</sub> at room temperature.

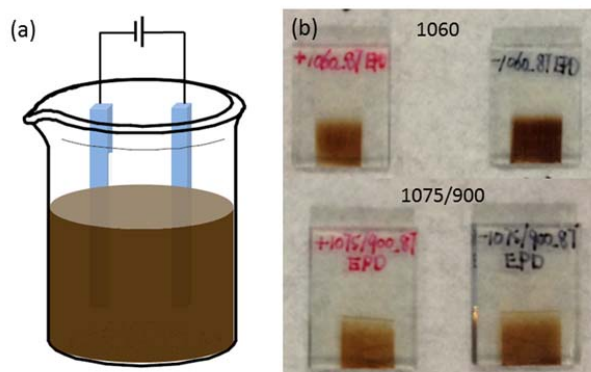


**Figure 2.3** (a) Illustration of the EPD system; (b) images of QDs/TiO<sub>2</sub> electrodes after 1 h of EPD, red and black labels corresponding to samples produced from positive and negative electrode of applied bias.

## 2.3 Characterizations

### 2.3.1 Scanning Electron Microscopy (SEM)

SEM is a type of electron microscope that generates a variety of signals at the surface of a specimen by scanning it with a focused beam of high-energy electrons. The

signals that derive from electron-sample interactions reveal information about the sample including external morphology, chemical composition, and crystalline structure and orientation of materials making up the sample. Typically, SEM consists of an electron optical column, a vacuum system, electronics and software. In principle, when a sample is bombarded with an incident electron beam, a variety of signals are generated. The three signals which provide the greatest amount of information in SEM are the secondary electrons, backscattered electrons and X-rays. Among them, secondary electrons are emitted from the atoms occupying the top surface and produce a readily interpretable image of the surface. The contrast in the image is determined by the sample morphology. In our experiment, the images of the samples were recorded using a field emission SEM (FESEM, JEOL JSM7401F) at an acceleration voltage of 5 kV. Cross section images were taken from a freshly cleaved cross-section of TiO<sub>2</sub> film. Compositional analysis was acquired using an Atmospheric Thin Window (ATW) energy dispersive EDX detector in FEI Sirion high resolution scanning electron microscope (HRSEM) system operated at 10-15 kV accelerating voltage, whose resolution is 133 eV at 5.9 keV.

### **2.3.2 Transmission Electron Microscopy (TEM)**

TEM is a type of electron microscopy technique that produce images with the interaction of a beam of electrons with an ultra-thin specimen. Owing to the small de Broglie wavelength of electrons, TEMs are capable of imaging at a significantly higher resolution than light microscopes. By showing different types of diffraction patterns such as dots, regions or circles that originate from the irradiated area of the sample, the information about local structure, average structure and chemical composition can be collected almost simultaneously. In our experiment, a JEOL 2100F TEM is not only used to directly observe the morphology and size of QDs dispersion but also used to analyze the morphology of QDs before and after grafting to TiO<sub>2</sub>.

### **2.3.3 X-ray Photoelectron Spectroscopy (XPS)**

XPS is a quantitative spectroscopic technique that measures elemental composition of the surface, the empirical formula of pure materials, and chemical and electronic

state of the elements in the surface and the thickness of thin film on a different substrate within the probing depth ( $\sim 10$  nm of the surface). A typical XPS spectrum is a plot the number of detected photoelectrons versus the binding energy of the electrons detected. The energy of the photoelectrons basically characterize the element and configure the electrons inside the atom such as 1s, 2s, 2p, 3s etc. Here, XPS was performed on a VG Escalab 220i-XL equipped with hemispherical analyzer recorded for a Twin Anode X-Ray Source. The spectra acquisition parameters (channel exposition, number of scans, analyzer parameters, etc.) were selected to provide the best energy resolution and signal/noise ratio. Pb 4f and C 1s photoelectron lines were acquired during the experiment. The C 1s peak (BE = 284.6 eV) was used as an internal reference line to accurately determine the positions of the other spectral lines. The fine structure of the photoelectron lines was treated using Casa XPS software (2.3.15 Version).

#### 2.3.4 Rutherford backscattering spectroscopy (RBS)

RBS is technique used to determine the composition and structure of materials by measuring the backscattering of a beam of high energy ions (typically protons or alpha particles) impinging on a sample at a well known energy. Rutherford backscattering can be described as an elastic (hard-sphere) collision between a high kinetic energy particle from the incident beam (the *projectile*) and a stationary particle located in the sample (the *target*). Typically, the energy loss of a backscattered ion is dependent on two processes.

The first energy loss process is the energy lost in scattering events with sample nuclei, which is dependent on the scattering cross-section of the nucleus and thus on its mass and atomic number. Nuclei of two different elements will therefore scatter incident ions to different degrees and with different energies for a given measurement angle, producing separate peaks on an  $N(E)$  plot of measurement count versus energy. These peaks are characteristic of the elements contained in the material, providing a means of analyzing the composition of a sample by matching scattered energies to known scattering cross-sections. Relative concentrations can be determined by measuring the heights of the peaks.

The second energy loss process is the energy lost to small-angle scattering from the sample electrons. The stopping power of the sample electrons creates a gradual energy loss which is dependent on the electron density and the distance traversed in the sample. This energy loss will lower the measured energy of ions which backscatter from nuclei inside the sample in a continuous manner dependent on the depth of the nuclei. The result is that instead of the sharp backscattered peaks one would expect on an  $N(E)$  plot, with the width determined by energy and angular resolution, the peaks observed trail off gradually towards lower energy as the ions pass through the depth occupied by that element. Elements which only appear at some depth inside the sample will also have their peak positions shifted by some amount which represents the distance an ion had to traverse to reach those nuclei.

An RBS instrument generally includes three essential components: An ion source, usually alpha particles ( $\text{He}^{2+}$  ions) or, less commonly, protons. A linear particle accelerator capable of accelerating incident ions to high energies, usually in the range 1-3 MeV. A detector capable of measuring the energies of backscattered ions over some range of angles. In practice, a compositional depth profile can be determined from an RBS  $N(E)$  measurement. The elements contained by a sample can be characterized from the positions of peaks in the energy spectrum. Depth can be determined from the width and shifted position of these peaks, and relative concentration from the peak heights. This is especially useful for the analysis of a multilayer sample or for a sample with a composition which varies more continuously with depth.

To investigate the dynamic of EPD, RBS was carried out using a  $4\text{He}^+$  beam under the following experimental conditions:  $E_0 = 5.1$  MeV; beam geometry: IBM; normal incidence of the beam on sample surface; scattering angle  $\theta = 140^\circ$ . RUMP Code was used to simulate the RBS spectra. The density of the  $\text{TiO}_2$  mesoporous films was calculated by dividing their areal density (defined as the number of atoms per surface area of the sample, obtained from RBS) by their thickness, measured through a stylus profilometer.

### **2.3.5 UV-visible (UV-vis) Spectroscopy**

A UV-vis spectrophotometer refers to absorption spectroscopy or reflectance spectroscopy in the ultraviolet-visible spectral region using light in the visible and adjacent (near - UV and NIR) ranges. Ultraviolet (190 - 380 nm) and visible (380 - 750 nm) radiation interacts with matter may cause promotion of electrons from the ground state to a high energy state, which also called electronic transitions. The UV-visible absorption spectrum was carried out for investigating the optical energy gap of the QD based on its optically induced transition. QDs were dispersed in toluene to acquire absorption spectra using a Cary 5000 UV-visible-NIR spectrophotometer (Varian) with a scan speed of 600 nm/minute. All experimental data were corrected for background absorption by toluene.

### **2.3.6 Photoluminescence (PL) Spectroscopy**

Photoluminescence spectroscopy is a non-contact, nondestructive method of probing the electronic structure of materials. In essence, light is directed onto a sample, where it is absorbed, a process called photo-excitation can occur. Then the material can jump to a higher electronic state, and will then release energy (photons) as it relaxes and returns to back to a lower energy level. The emission of light, or luminescence through this process is photoluminescence, PL. Analysis of PL helps to identify surface, interface and impurity levels and understand the underlying physics of the recombination mechanism. In our experiment, steady state PL spectroscopy of samples were taken with a Fluorolog®-3 system (Horiba Jobin Yvon) using an excitation wavelength of 670 nm.

### 3. DYNAMICS OF QD UPTAKE INTO MESOPOROUS $\text{TiO}_2$ THICK FILMS THROUGH EPD

#### 3.1 Synthesis and characterization of QDs in solution and in $\text{TiO}_2$ films

Colloidal PbS QDs and PbS@CdS QDs of diameters ranging between 2.9 - 4.1 nm were synthesized and then dispersed in toluene, with typical QY of 40 ~ 80%. We selected three different sizes of QDs:  $3.0 \pm 0.3$  nm,  $3.6 \pm 0.3$  nm,  $4.0 \pm 0.3$  nm and compared pure PbS and PbS@CdS core@shell QDs with similar diameters (the representative size distribution for samples PbS\_M and PbS@CdS\_M are shown in **Figure 3.1**).

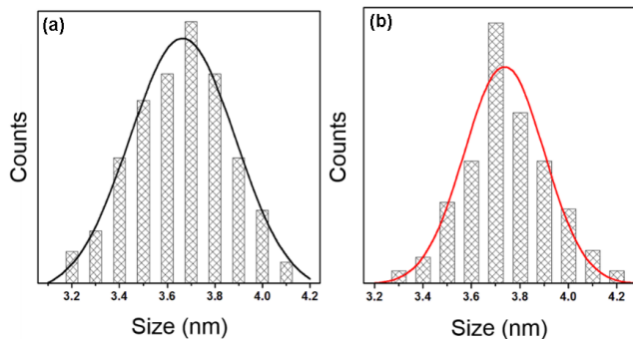


**Figure 3.1** Size distributions of (a) PbS\_M and (b) PbS@CdS\_M QDs.

The absorption spectra of samples with different sizes of PbS and PbS@CdS QDs in toluene are shown in **Figure 3.2** (a). The average PbS diameter for PbS QDs and the average PbS core size for the core@shell QDs are determined from the position of the first-lowest energy excitonic absorption peak (see Equation 1.1). [91] CdS shell thickness in PbS@CdS QDs can be obtained by simple subtraction from the overall size of PbS@CdS QDs based on TEM observations and the PbS core size. Based on previous achievements, [90] the shell of PbS@CdS QDs is mainly composed of CdS. The overall QD diameter ( $d_{\text{total}}$ ), core diameter ( $d_{\text{core}}$ ), CdS shell thickness ( $d_{\text{shell}}$ ), the position of the first excitonic absorption peak and PL peak are listed in **Table 3.1**.

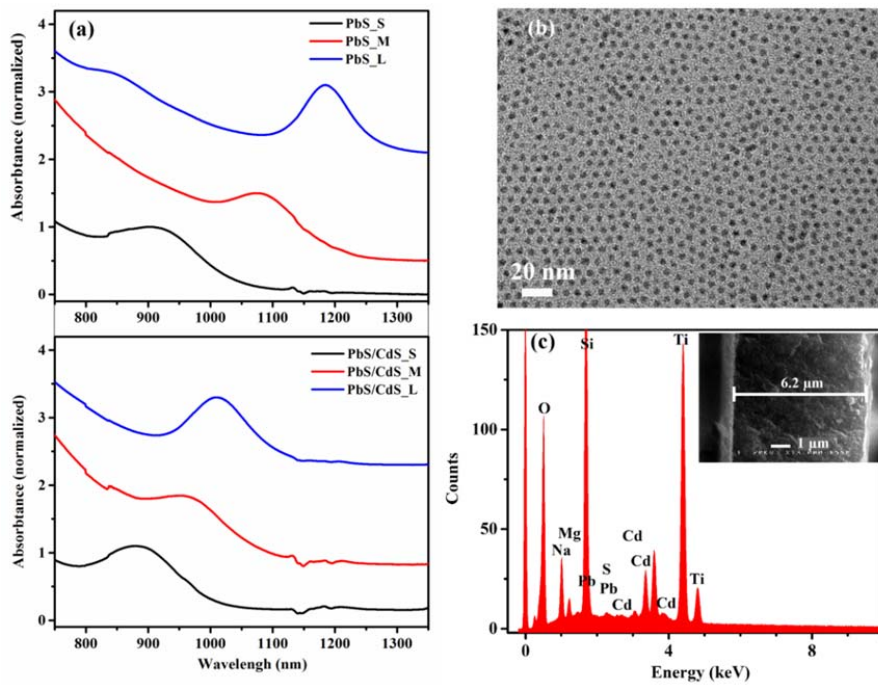


**Figure 3.2** Absorption spectra of (a) PbS and PbS@CdS QDs in solution. (b) Representative TEM image of PbS@CdS QDs. (c) EDX analysis of PbS@CdS QDs with ~3.0 nm core diameter (shell thickness ~0.2 nm) after anchoring to TiO<sub>2</sub> nanoparticles by using EPD for 30 min (negative TiO<sub>2</sub> electrode). Inset: SEM cross-section of a TiO<sub>2</sub> film.

**Table 3.1** Dimensions and optical properties of pure and core@shell QDs investigated in this study. The overall size of PbS@CdS QDs is determined based on TEM observation, the core size is estimated from the position of the first excitonic peak and the shell thickness is estimated by simple subtraction. To identify the different samples, S M L labels are used according to their small, medium and large size, respectively.

Sample	Diameter (nm)	Core Diameter (nm)	Shell thickness (nm)	Abs max (nm)	PL max (nm)
PbS_S	3.09±0.3	3.09	0	912	
PbS_M	3.69±0.3	3.69	0	1079	
PbS_L	4.11±0.3	4.07	0	1184	
PbS@CdS_S	3.12±0.3	2.98	0.07	879	920
PbS@CdS_M	3.68±0.3	3.26	0.21	961	1075
PbS@CdS_L	4.10±0.3	3.44	0.33	1012	1180

As-synthesized QDs were then loaded into mesoporous TiO<sub>2</sub> layers through EPD. TiO<sub>2</sub> film thickness was around ~6 μm, estimated through stylus profilometer. SEM cross-section was also carried out on selected samples (see Figure 3.2 (c)) to compare

the values between profilometry and SEM, which agreed within the experimental errors. After EPD of QDs, both the positive and negative  $\text{TiO}_2$  electrodes were colored (Figure 2.3 (b)), consistently with previous studies, [63, 78] indicating the deposition of negatively and positively charged QDs. According to literature, [92] the initial positive charge in nanocrystals can be understood in terms of the preferential removal of ligand, which exposes Pb (or Cd for core@shell) sites at the surface, which may also make QDs more “sticky” by reducing the solubilisation energy in the solvent, and may help charge transfer at the electrode surfaces. The origin of the negatively charged nanocrystals, can be explained with a S-rich surfaces or surface reconstruction upon the loss of the passivating ligand molecules, which exposes S atom. [93, 94] We investigated both positive and negative  $\text{TiO}_2$  electrode, presenting almost the same results. Here we just show the investigation on negative  $\text{TiO}_2$  electrode. The effective deposition of QDs into the  $\text{TiO}_2$  is confirmed by the EDX, Figure 3.2 (c) in SEM (inset of Figure 3.2 (c)), in which the signal from Cd, Pb and S are clearly visible.

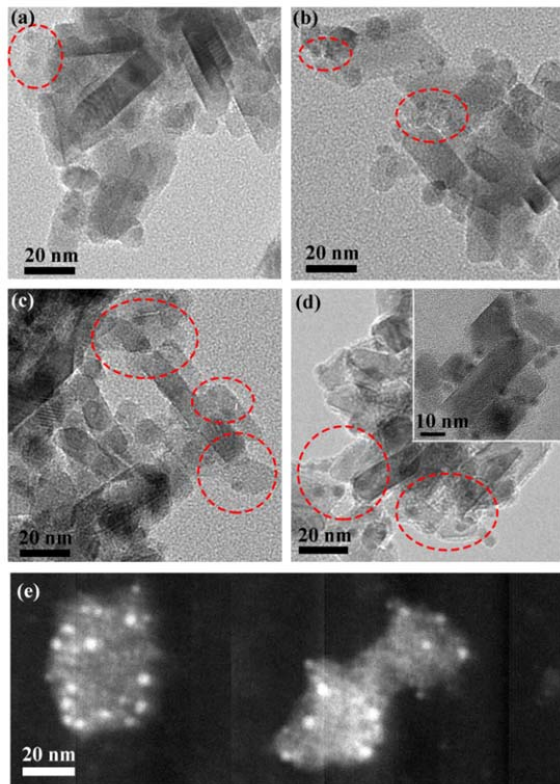


**Figure 3.3** Representative TEM images of  $\text{PbS}@\text{CdS}$  QDs loaded into  $\text{TiO}_2$  at four different EPD durations (negative  $\text{TiO}_2$  electrode): (a) 10 min (b) 30 min (c) 60 min (d) 120

min. Inset of (d): enlarged TEM image. The red circles highlight the presence of the QDs. (e) Dark field Scanning TEM image of  $\text{TiO}_2$  nanoparticles covered by QDs. The high contrast between the  $\text{TiO}_2$  and QDs allow precise identification of the position of the QDs on the surface of  $\text{TiO}_2$  nanoparticles.

**Figure 3.3** collects TEM images of negative  $\text{TiO}_2$  electrodes sensitized with  $\text{PbS@CdS}$  core@shell QDs at different EPD durations.  $\text{TiO}_2$  coverage becomes denser at increasing EPD time (Figure 3.3 (d)). In summary, the EPD process produces well-separated core@shell QDs, without obvious QD aggregation occurs, which could be detrimental for electron transfer in the operating device.

## 3.2 QD Stability after EPD

To check the effect of EPD on the stability of the structure and optical properties of QDs, we performed XPS and PL analyses of selected QDs deposited on silicon substrate or after EPD on  $\text{TiO}_2$  mesoporous films. We compared QDs with and without CdS shell to test the ability of the shell to prevent QD degradation.

XPS was used to characterize the effect of EPD on the chemical bonds in QDs. The results are collected in **Figure 3.4**. The high-resolution spectrum of Pb 4f in  $\text{PbS}$  QDs on silicon reveals the presence of Pb 4f 7/2 (137.9 eV) and Pb 4f 5/2 (142.7 eV), respectively, from Pb-S bonds, and also two higher energy components (138.5 eV for Pb 4f 7/2 and 143.3 eV for Pb 4f 5/2), which can be originated from the interaction between Pb and OA ligands. [91] After EPD, the high energy peaks of Pb 4f totally disappear, and two additional lower energy components appear at 136.6 eV for Pb 4f 7/2 and 141.4 eV for Pb 4f 5/2 of  $\text{PbS}$  (Figure 3.4 (a)), which might be attributed to the presence of Pb dangling bonds due to the unpassivated Pb atoms on the QD surface, as a result of EPD. [91] The interaction between the QDs and  $\text{TiO}_2$  NPs might be the reason for the shift of Pb-S bond to higher energies, from 137.9 eV to 138.1 eV for Pb 4f 7/2 and from 142.7 eV to 142.9 eV for Pb 4f 5/2. The high resolution spectrum of Pb 4f in  $\text{PbS/CdS}$  QDs on silicon (Figure 3.4 (b)) presents two additional higher binding energy peaks, similar to  $\text{PbS}$  QDs on silicon, slightly less intense than in  $\text{PbS}$  QDs. This feature possibly implies the presence of interaction between a small amount of unpassivated Pb atoms on the QD surface and ligands, as well as oxygen in aerobic

environments. In fact, some of PbS@CdS QDs might have an incomplete CdS shell, leaving some portion of Pb atoms at the surface. After EPD, in contrast to pure PbS, the two additional higher binding energy peaks almost maintained the same position as those on silicon, indicating increased damage in pure PbS QDs, while, for core@shell structure, there is no indication of formation of dangling bonds, and a relatively better structural stability.

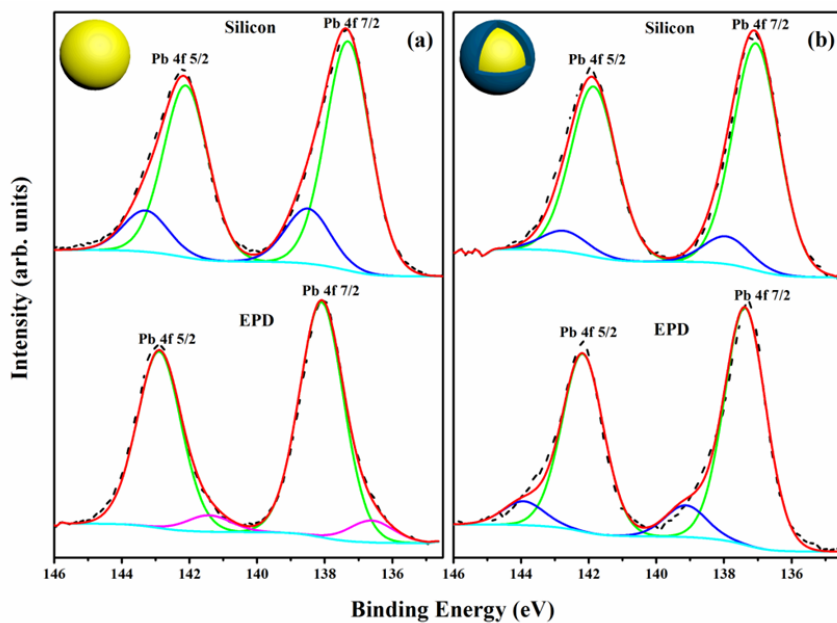


**Figure 3.4** High resolution Pb 4f core level spectra Photoelectron spectra after correction of electrostatic charging obtained from (a) PbS\_M quantum dot (b) PbS@CdS\_M core@shell quantum dot on silicon (up) and upload into  $\text{TiO}_2$  with EPD (down).

PL spectra of  $\text{TiO}_2$  samples after EPD of PbS and PbS@CdS QDs, 3.6 nm in size, are reported in **Figure 3.5** (a) and (b), respectively. Quantum confinement in QDs results in size-dependent band gap, inducing size dependent PL. The PL peak position of pure PbS QDs after EPD (1175 nm) has a blue shift (32 nm) compared to pure PbS in solution (1207 nm), indicating the shrinking of QDs during uptake. After 24 hours exposure to air, the PL peak position further blue shifts ( $\sim$ 138 nm) compared to pure PbS QDs in solution, probably due to PbS oxidation. In fact, oxidation reduces the size of un-oxidized PbS, which is the source of PL, thus causing blue shift of PL signal due to the shrink of the emitting PbS volume. In addition, the peak width is quite broad ( $\sim$ 212 nm) with respect to that in solution ( $\sim$ 141 nm), indicating the presence of trap-related

emission, consistently with the presence of un-passivated dangling bonds confirmed by XPS (Figure 3.4 (a)). In PbS@CdS core@shell QDs, almost no shift of the PL peak was recorded, even after exposing the sample to air for 24 h (Figure 3.5 (b)), clearly demonstrating the increased optical stability thanks to the presence of the passivating shell.

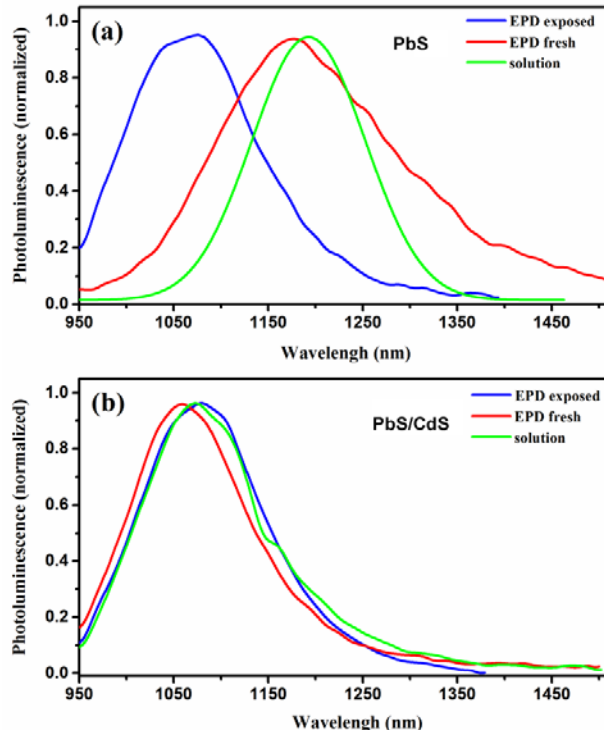


**Figure 3.5** PL of (a) PbS\_M QDs and (b) PbS@CdS\_M QDs just after EPD and after 24 hours exposure to air. Benchmarking PL spectra of QDs in solution is also reported.

### 3.3 Dynamics of EPD

The increased stability of core@shell QDs motivated us to select this structure to investigate the dynamics of QDs uptaken during EPD. We applied RBS to get information on depth profiling of QDs inside the TiO<sub>2</sub> matrix. The RBS spectrum of a typical sample after EPD is reported in **Figure 3.6**.

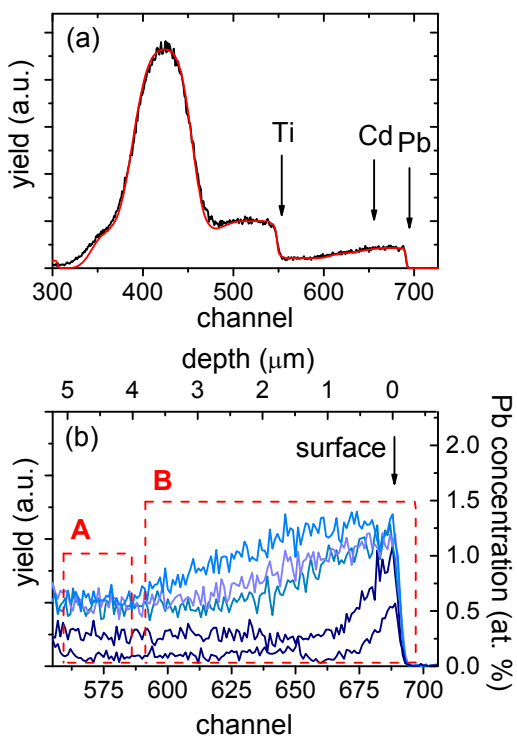


**Figure 3.6** (a) RBS spectrum of  $\text{TiO}_2$  mesoporous film sensitized with QDs for 120 minutes. The red curve is the RUMP code simulation. The surface edges for Ti, Cd and Pb are indicated by arrows. (b) RBS signal of the spectral region pertaining Pb signal for samples sensitized at different durations (5, 10, 30, 60, 120 minutes, from dark blue to light azure). A and B rectangles highlight the two different regions in which QD diffusion cannot be detected (A) or is clearly visible (B).

The signals from Ti and Pb are clearly visible, allowing quantitative analysis of in-depth distribution of Pb into the  $\text{TiO}_2$  layer. The red curve is the RUMP code simulation, including also the contribution from FTO substrate, demonstrating that very accurate depth profiling of Pb is possible in this kind of samples. The signal from Cd is masked by Pb, can be hardly detected, and is very close to the detection limit of the technique in the present experimental conditions. For this reason, we focused on the depth profiling of Pb, under the hypothesis that the core@shell structure and Pb:Cd atomic ratio is preserved after EPD and so, in principle, Cd depth profile is the same as Pb.

Figure 3.6 (b) focuses on the RBS spectral range related to Pb. Two different regions can be clearly identified: region A, relying with the inner part of the film at the  $\text{TiO}_2$ /FTO interface, and region B, which represents the exterior part of the film, close to the

surface. In region A, the concentration of Pb is almost constant and depth-independent, and increases exponentially with EPD time (see **Figure 3.7**).

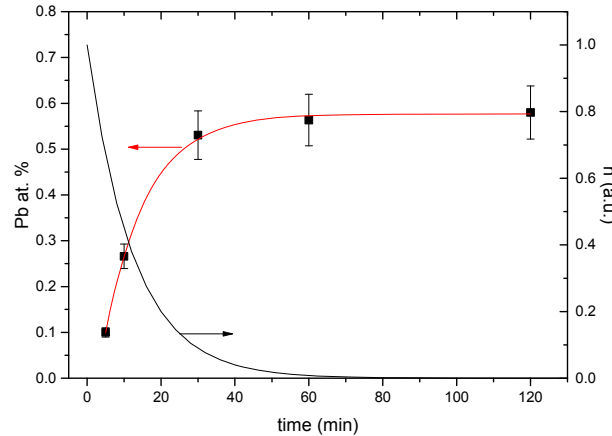


**Figure 3.7** Pb atomic ration as a function of EPD time at the interface of  $\text{TiO}_2/\text{FTO}$  for  $\text{PbS}@\text{CdS}_\text{L}$  (red line) Black line corresponding to the change of the curvature.

Pb is present even at very short EPD time, indicating that the solution containing QDs penetrates the entire film depth from the beginning of the process and that QD start attaching to  $\text{TiO}_2$  over the entire depth of the film. In region B, a surface Pb peak is present after 5 min EPD deposition. Then Pb penetrates the film during EPD. Pb surface concentration increases with the time up to a saturation concentration (see **Figure 3.8**).

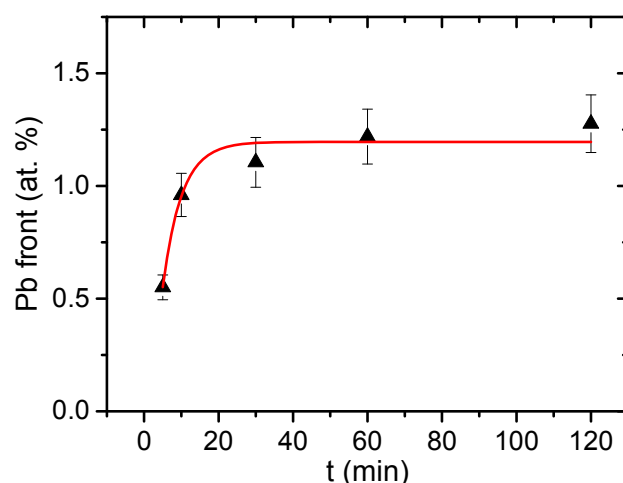


**Figure 3.8** Pb atomic ration as a function of EPD time at the surface of  $\text{TiO}_2$  film of  $\text{PbS}@\text{CdS}_\text{L}$

We calculated the main Pb parameters as a function of EPD time from RBS spectra: (i) Pb atomic concentration at the surface (surface peak in region B); (ii) Pb atomic concentration at the interface with FTO (from region A); (iii) penetration depth of Pb ( $x_0$ , presented in **Figure 3.9** (a)). Being  $C(x,t)$  the atomic concentration of Pb as a function of the position inside the film and  $t$  the EPD time, and being  $C_s(t)$  and  $C_i(t)$  Pb atomic concentration at the surface of the film and at the FTO/TiO<sub>2</sub> interface, respectively,  $x_0$  is defined as:

$$C(x_0, t) - C_i(t) = \frac{C_s(t) - C_i(t)}{2} \quad \text{Equation 3.1}$$

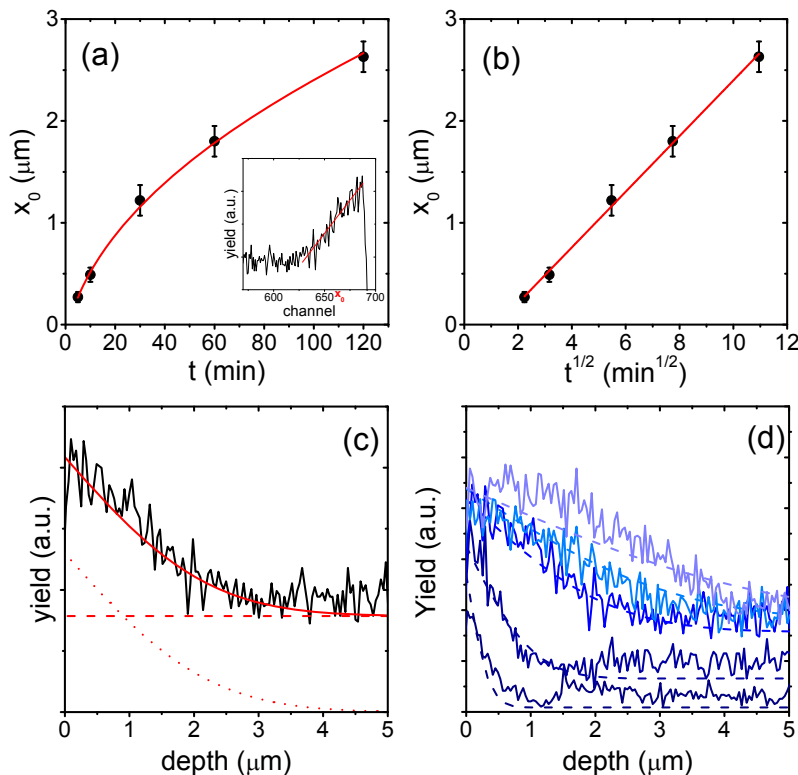


**Figure 3.9** (a) Position of the parameter  $x_0$  as a function of EPD time. Inset: illustration of the procedure to determine  $x_0$  from a standard RBS spectrum. (b) Parameter  $x_0$  versus square root of EPD time. (c) Experimental Pb yield (black line) versus film depth and simulated yield (red solid line) obtained from the diffusion coefficient  $D$  and the characteristic decay time  $\tau$  obtained from RBS data. The two different components contributing to the curve are reported: diffusion process of Pb from solution (red dotted line) and position-independent QD uptake (red dashed line). (d) Experimental (solid lines) and simulated (dashed lines) Pb yields for the complete series of EPD samples.

Figure 3.9 (a) and (b) report  $x_0$  as a function of the EPD time and square root of EPD time, respectively. The parameter  $x_0$  exhibits linear dependence on the square root of the EPD time. Such dependence is typical of diffusion processes driven by Fick's diffusion, [95] in which the penetration depth presents a square root dependence on diffusion time and is regulated by a diffusion coefficient  $D$ , according to the following:

$$\frac{C(x_0, t) - C_i}{C_s - C_i} = 1 - \text{erf}\left(\frac{x}{2\sqrt{Dt}}\right) \quad \text{Equation 3.2}$$

In a typical Fick's diffusion (see *Equation 3.2*), the parameters  $C_i$  and  $C_s$  are time-independent, being the concentration of the diffusing element constant at the surface source and in the bulk at infinite distance from the surface. [95]

However, in the present case, both  $C_i$  and  $C_s$  are dependent on EPD time, as clearly visible from the experiment, not allowing straightforward application of Fick's second law to EPD. In addition, the process under investigation is not a simple diffusion process, since our system is composed of various elements, mutually interacting: the solution, in which QDs are dispersed; the  $\text{TiO}_2$  host in which QDs can attach; the external electric field, which provides QD attachment. Furthermore, we are not detecting the QDs diffusing in the solution, but the QDs attached to the oxide. For all these reasons, the explanation of the experimental results needs a few assumptions on the physical chemical processes taking place during EPD.

At the beginning of the EPD, QD concentration is constant inside the solution penetrated into the mesoporous film. Application of the external electric field induces attachment of QDs to  $\text{TiO}_2$ . This process causes the decrease of QD concentration in the solution permeating the  $\text{TiO}_2$  mesoporous layer, while QD concentration outside  $\text{TiO}_2$  film keeps constant. We quantitatively estimated the decrease of QD concentration in the solution permeating the film from the amount of Pb in region A of the RBS spectrum: as already mentioned, Pb concentration in region A exhibits an exponential growth up to an asymptotic limit (Figure 3.7). The characteristic time of the process is  $\tau = (11.5 \pm 0.5)$  min. We interpret the asymptotic Pb concentration due to the full depletion of the solution from QDs. In fact, TEM results (Figure 3.3 clearly show that  $\text{TiO}_2$  coverage is not complete and Pb concentration in region B (higher than in region

A) demonstrates that further QD uptake is possible, if enough QD are present in solution. In addition, EPD tests at different voltages indicate that the asymptotic Pb concentration is almost independent on the applied electric field, within the experimental error (see **Table 3.2**), supporting once again the hypothesis of complete QD depletion of the solution inside the film in the first minutes of EPD.

**Table 3.2 PbS concentration and diffusion coefficient D as a function of the applied voltage in EPD.**

Applied voltage (V)	Pb at.% (surface)	Pb at.% (interface)	D ( $10^{-3} \mu\text{m}^2 \text{s}^{-1}$ )
50	1.20±0.1	0.55±0.05	(1.1±0.3)
100	0.95±0.05	0.50±0.05	(0.12±0.03)
200	0.60±0.05	0.40±0.05	(0.015±0.004)

The decrease of QD concentration inside the solution contained in the  $\text{TiO}_2$  film creates a concentration gradient that induces QD diffusion from the solution outside the film, into the solution inside the film. Once the QDs enter the film, they can attach to  $\text{TiO}_2$  surface due to the action of the electric field.

An empirical description of Pb concentration as a function of EPD time and of the position inside the film assumes that the process of QD uptake at the beginning of EPD, and the process of QD diffusion due to the rise of QD concentration gradient are mutually independent.

Under this hypothesis, the concentration  $C(x,t)$  can be written as follows:

$$C(x,t) = C_0 \left[ 1 - \exp\left(-\frac{t}{\tau}\right) \right] + C_1 \left[ 1 - \operatorname{erf}\left(\frac{x}{2\sqrt{Dt}}\right) \right] \quad \text{Equation 3.3}$$

The first part accounting for position-independent QD uptake from original solution and the second part taking into account QD diffusion from the surface and successive QD uptake. Of course, this assumption oversimplifies the problem, since the two processes are correlated. However, the agreement between the proposed solution and

the experimental findings is quite impressive, as visible in Figure 3.9 (d), in which the experimental data (solid lines) are interpolated using *Equation 3.3* (dashed lines).

In the interpolation,  $C_0$ ,  $\tau$ ,  $C_1$ , and  $D$  are experimentally determined.  $C_0$  is the asymptotic Pb concentration in region A after 120 minutes EPD,  $\tau$  is calculated from the Pb atomic concentration in region A as a function of the time (Figure 3.7),  $C_1$  is the asymptotic Pb concentration at the surface of  $\text{TiO}_2$  film, and  $D$  is the diffusion coefficient calculated from the linear fit of Figure 3.9 (b).

A reconstruction of Pb depth profiling versus EPD time is reported in **Figure 3.10**, based on *Equation 3.3*. The concentration gradient created at the surface, due to the depletion of solution inside  $\text{TiO}_2$  is well visible, as well as the evolution of PbS depth profile leading to the final concentration after long EPD.

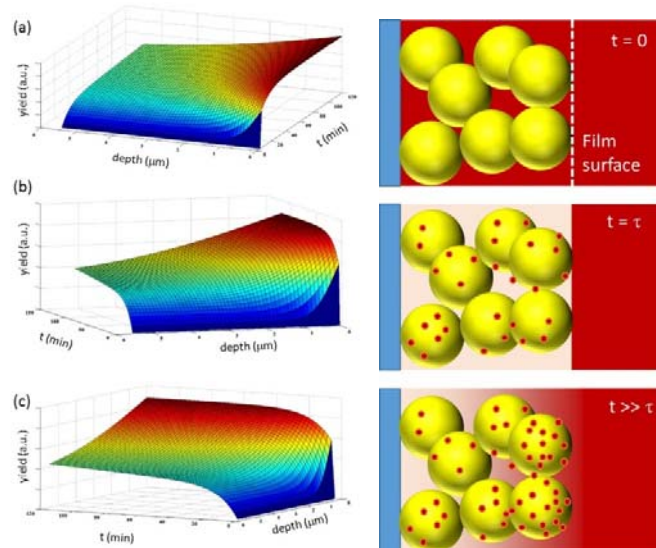


**Figure 3.10** Pb distribution versus time and depth in  $\text{TiO}_2$  film under three different perspectives, based on the experimental parameters calculated for 200 V applied bias.

We extended the investigation of EPD to different applied voltages. **Figure 3.11** shows the parameter  $x_0$  versus the square root of EPD time (Figure 3.11 (a)), the diffusion coefficient versus EPD bias (Figure 3.11 (b)), and the fitting of three Pb profiles after 60 min EPD at three different voltages (Figure 3.11 (c)). For all the applied biases,

$x_0$  exhibits linear dependence on the square root of the EPD time, the slope increasing at increasing bias. Accordingly,  $D$  is dependent on the applied voltage and, in particular, it increases from  $(1.5 \pm 0.4) \times 10^{-5} \mu\text{m}^2 \text{s}^{-1}$  at 50 V to  $(1.1 \pm 0.3) \times 10^{-3} \mu\text{m}^2 \text{s}^{-1}$  at 200 V. The increase in  $D$  reflects in Pb depth profiling, as it is visible in Figure 3.11 (c), in which Pb profile is reported for three different voltages after 60 mins EPD. The interpolating curves after 60 mins EPD were based on the experimental results on  $C_i$ ,  $C_s$  and  $\tau$  as reported in Table 3.2.

Of course, in detection of Pb through RBS it is impossible to give an exhaustive description of the process of QD motion inside the film and of QD grafting, separately, since the signal from Pb relies with QDs after grafting. It means that the information about QD motion inside the film is mediated by the process of QD attachment, under the hypothesis that the characteristic time for grafting does not depend on QD concentration. However, there may be a dependence of the characteristic grafting time with the applied voltage, but we are not able to discriminate this dependence and the dependence of QD motion.

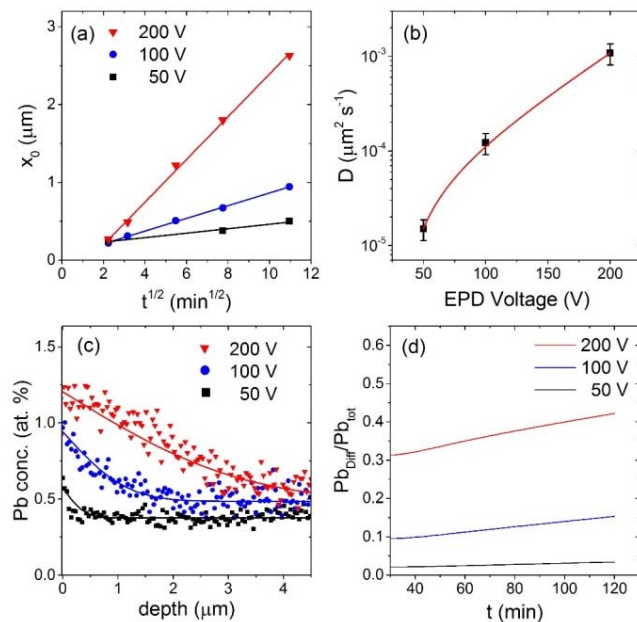


**Figure 3.11** (a)  $x_0$  versus square root of EPD time. (b) Diffusion coefficient  $D$  versus EPD voltage, and (c) Pb concentration versus depth at three different EPD voltages after 60 min EPD. Symbols: experiment; solid lines: simulations according to the values of  $D$  reported in Table 3.2 (d) Fraction of Pb introduced in the film by diffusion ( $Pb_{\text{diff}}$ ) and the total Pb amount are calculated as the

**integral of Pb concentrations along film depth based on the two components illustrated in Figure 3.9 (c).**

In addition, the previous achievements allow us, by simple integration, to determine the quantity of Pb entering  $\text{TiO}_2$  at the beginning of the process through the pristine solution, and the quantity of Pb diffusing from the external solution inside the film. The fraction of Pb entering the film due to diffusion is reported in Figure 3.11 (d) for three different applied voltages as a function of EPD time. As can be readily seen, application of 50 V induces negligible diffusion, and the amount of QD is almost due to QD uptake directly from the pristine solution. As soon as the applied voltage increases, the fraction of Pb coming from diffusion increases. At 200 V, after 120 mins of EPD, more than 40% of the Pb decorating the  $\text{TiO}_2$  comes from diffusion from the external solution, indicating that this process cannot be neglected during the preparation of this kind of composite systems.

## 4. PROMISING APPLICATIONS

The special property of QDs and quantitative optimization of QD sensitized mesoporous films can provide enormous opportunities for practical applications, such as PV devices and PEC H<sub>2</sub> production. Here, we have developed hybrid architecture of photoanode based on a TiO<sub>2</sub> mesoporous frame, functionalized with colloidal core@shell PbS@CdS QDs, followed by CdS capping via SILAR for passivation and light absorption, targeting an efficient and stable QD sensitized photoanode. A blocking layer was placed between the mesoporous TiO<sub>2</sub> and FTO, to prevent recombination of electrons in the FTO with the oxidized species in the electrolyte. [96] After mesoporous TiO<sub>2</sub> thin film was deposited on TiO<sub>2</sub> blocking layer, the as-synthesized QDs dispersed in toluene were tightly anchored with the surface of TiO<sub>2</sub> nanoparticles by EPD guaranteeing the efficient electron transfer from the photoexcited QDs to TiO<sub>2</sub>. Thanks to the shell of colloidal QDs, the PbS core was escaped from surface oxidation so that the long-term photostability of the device was enhanced. [97] The preliminary tests in the following directions have been proved promising and further investigations could be fruitful.

### 4.1 QDSCs fabrication

Based on the previous work on the successful preparation QD sensitized photoanodes, QDSCs can be further fabricated and the device strcuture is schematically illustrated in **Figure 4.1**. The polysulfide electrolyte aqueous solution consists of 0.5 M Na<sub>2</sub>S, 2 M S, and 0.2 M KCl in methanol/water (7 : 3 / v : v) following the work by Lee and Chan. [98] The whole electrical circuit is closed by Cu<sub>2</sub>S counter electrode, which was prepared by immersing brass into 0.5 M HCl at 70 °C for 30 minutes followed by a 1 M Na<sub>2</sub>S/1 M S (polysulfide) solution for 10 minutes, then dried with a N<sub>2</sub> gun.

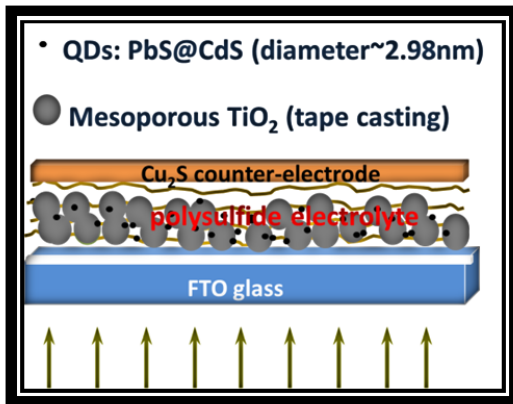


**Figure 4.1 Scheme of the QDSCs.**

The current–voltage profile of QDSCs fabricated by using EPD is illustrated in **Figure 4.2**. A efficiency around 0.42 % was yield while the  $V_{oc}$  was 0.3V (Voc is around 0.55 V or even lower, in most of the cases, when polysulfide electrolyte is used). Therefore the increase in Voc is the main current challenge to increase the efficiency of QDSCs. In general, the fundamental process determining  $V_{oc}$  is recombination, and the dark saturation current can be considered a direct measure of the recombination in the PV device. There are three possible fundamental sources of voltage loss: charge transfer activation or “kinetic” losses, ion and electron transport or “ohmic” losses, and concentration or “mass transfer” losses. Among other factors, further investigation on voltage loss need to be done with Electrochemical Impedance Spectroscopy (EIS), which is an experimental technique that can be used to separate and quantify these sources of polarization. By applying physically-sound equivalent circuit models wherein physiochemical processes occurring within the cell are represented by a network of resistors, capacitors and inductors, we can extract meaningful qualitative and quantitative information regarding the sources of impedance within the cell.

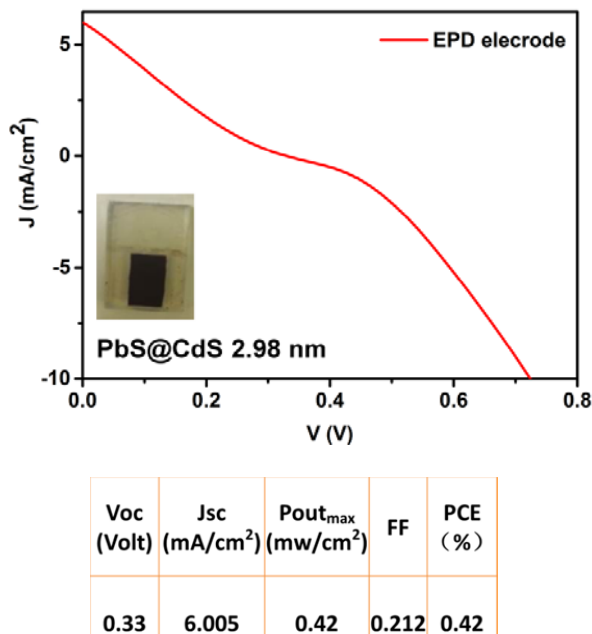


**Figure 4.2** J-V characteristics of QDSCs fabricated with PbS@CdS QDs-decorated TiO<sub>2</sub> (device was coated with CdS and ZnS) under AM1.5G illumination with light intensity of 100 mW/cm<sup>2</sup>.

## 4.2 Water splitting

Our previous study already demonstrated that PbS@CdS core@shell QDs exhibit much increased long-term stability toward oxidation compared to their pure PbS counterpart. QD can deposit into mesoporous TiO<sub>2</sub> film with uniformed coverage under quantitative control over whole EPD process, indicating they are strong candidates for the development of highly efficient and stable light absorbers, which is ideal PEC H<sub>2</sub> production.

PEC properties of TiO<sub>2</sub> decorated with PbS@CdS QDs were investigated using a cell with three-electrode configuration, which consists of an Ag/AgCl reference electrode, a Pt counter electrode, and an working electrode. An aqueous solution containing 0.24 M Na<sub>2</sub>S and 0.35 M Na<sub>2</sub>SO<sub>3</sub> (PH=13) as the sacrificial hole scavenger was used as the electrolyte to prevent photocorrosion of the QDs. The PEC cell was evacuated after pouring the electrolyte solution into the reactor. A 300 W xenon arc lamp with a long-pass filter was used as the light source and the working electrode was illuminated through a quartz window. An external bias between the electrodes was applied for

efficient charge separation, even the QD and  $\text{TiO}_2$  possesses a suitable conduction band energy level (higher than the potential of  $\text{H}_2/\text{H}_2\text{O}$ ) for reducing water to  $\text{H}_2$ , possibly due to the resistance produced between the two electrodes in the solution and to that produced at the interfaces between semiconductor particles within the electrode.

**Figure 4.3** (a) presented the PEC behavior of QD sensitized photoanode under AM 1.5G illumination ( $100 \text{ mW/cm}^2$ ). The observed positive photocurrents correspond to hole injection from the heterostructured  $\text{TiO}_2/\text{QDs}$  photoanode into the solution. Saturation of the photocurrent takes place at approximately 0.2 V versus the RHE, with  $8 \text{ mA}\cdot\text{cm}^{-2}$  for  $100 \text{ mW/cm}^2$  light intensity, equals  $80 \text{ mL}\cdot\text{cm}^{-2}\cdot\text{day}^{-1}$  hydrogen generation rates, assuming a faradaic efficiency of unity, which is the 30% higher than the PEC system using SILAR  $\text{PbS}@\text{CdS}$  QDs ( $60 \text{ mL}\cdot\text{cm}^{-2}\cdot\text{day}^{-1}$ ). [99] As shown in Figure 4.3 (a) and (b), when the light intensity reached to  $800 \text{ mW/cm}^2$  under AM 1.5G illumination, photocurrent density reaches to  $66 \text{ mA/cm}^2$  and the electrodes were still shown to be stable (no decrease of photocurrent during more than 10 min, Figure 4.3 (b)). The photocurrent is almost proportional to the light density, indicating that the photoanode keeps stable during the illumination even with high light intensity. This suggests that the photoanode show a very good stability benefiting from the  $\text{CdS}$  shell, which could isolate the  $\text{PbS}$  core to the environment effectively. The high intensity illumination stability makes it a good potential to work with solar concentrator, [100-102] which can concentrate a large area of sunlight, or solar thermal energy, onto a small area with high light intensity. In addition, the increasing temperature produced by solar thermal energy could decrease the necessary energy for electrolytic  $\text{H}_2$  production, [103, 104] as a consequence, the electrolysis of water could be substantially enhanced. The optimization strategies are under investigation using the luminescence solar concentrator in our lab to improve the device efficiency with long-term stability.

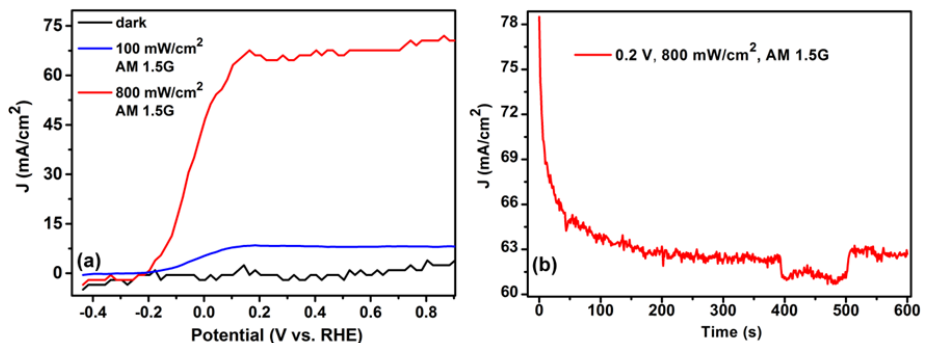


**Figure 4.3 (a) Photocurrent density versus the applied voltage referenced to RHE and (b) photocurrent responses at 0.2 V vs RHE of TiO<sub>2</sub>/colloidal QDs photoanode.**

## 5. CONCLUSION AND FUTURE PERSPECTIVES

### 5.1 Conclusion

In summary, we investigated the upload of NIR colloidal core@shell QDs into mesoporous TiO<sub>2</sub> films by EPD. We demonstrated good electrode coverage without QD aggregation and improved the stability of core@shell QDs towards oxidation and defect formation after EPD, compared to pure PbS QDs. We studied the dynamics of QD uptake through EPD via RBS. The entire process can be rationalized as follows: First, QD concentration is constant inside the solution penetrated into the mesoporous film, and the applied electric field induces attachment of QDs to TiO<sub>2</sub>. Then, depletion of QD in solution induces the formation of QD concentration gradient inducing a Fick's-like diffusion. The diffusion coefficient  $D$  exhibits a strong electric field enhancement, which is still not completely clear and needs to be further investigated. These results clearly demonstrate that QD uptake can be finely tuned by controlling the main EPD parameters, and give rational and quantitative description of the preparation of QD sensitized photoanodes for QDSCs and PEC H<sub>2</sub> production. These results can also be applied, in principle, to other kinds of semiconducting nanocrystals commonly applied for the sensitization of mesoporous electrodes.

## 5.2 Perspectives

Colloidal PbS@CdS QDs are appropriate materials for solar energy conversion and show promising developments for QDs sensitized photoanode. Future works should focus on:

1. EPD dynamic investigation:

The QD' diffusion coefficients within the TiO<sub>2</sub> films imbued with the deposition solution show high voltage dependence. Our analysis of the profiles based on the Fick's law alone (diffusion only) defined apparent diffusion coefficients. Our next step is to take transport under an electrical field into consideration. It could be interesting to consider the Nernst-Einstein relation between mobility and diffusion coefficient. From general considerations of transport in a force field, the diffusion constant D can be written as  $D = \mu k_B T$ , where  $\mu$  is the "mobility", or the ratio of the particle's terminal drift velocity to an applied force;  $k_B$  is Boltzmann's constant;  $T$  is the absolute temperature. For diffusion of charged particles<sup>105</sup> (*Principles of Semiconductor Devices* online textbook by Van Zeghbroeck, Chapter 2.7), the diffusion constant D can be described by electrical mobility equation  $D = \frac{u_q}{q} k_B T$  where  $u_q$  is the electrical mobility of the charged particle and  $q$  is the electrical charge of a particle. We would like to try to collect the information about the  $u_q$  and  $q$  during EPD so that we can apply Nernst-Einstein equation as next step to complete our simulation. A variation of the mobility of the drifting charges could explain at least in part the dependence of the (apparent) diffusion coefficients with the applied potential.

2. Optimization of experimental conditions to improve the performance of photoanode :

- 1) engineering the core size for wider wavelength range of optical absorption;
- 2) moderiating CdS shell thickness to optimize the charge transfer and stability;
- 3) constructing suitable EPD condition for photoelectrodes to load more QDs;
- 4) modifying TiO<sub>2</sub> scaffold film to decrease the charge recombination.

3. The development of PEC H<sub>2</sub> production by using the NIR core@shell QDs

- 1) engineering the CdS shell thickness to optimize the charge transfer and stability;
- 2) engineering the surface capping agents (such as halide) of core@shell QDs to improve the change transfer rate;
- 3) engineering the core size of QDs active even under wide infrared region;
- 4) annealing the photoanode after CdS coating to improve the charge transfer by removing the surface traps;
- 5) large-scaling solar H<sub>2</sub> of PEC with a long-term stability.
- 6) substantial improvements of this PEC system in the context of a stand-alone device combining a photovoltaic absorber unit for sunlight harvesting and electrocatalytic H<sub>2</sub> production with solar energy as the only energy source.

## 6. REFERENCES

- [1] U. Cubasch, G. A. Meehl. In Climate Change 2001: The Scientific Basis. Ed. J. T. Houghton, Cambridge Univ. Press, Cambridge, 2001, 525–582.
- [2] D. Wilson. We Have the Power; Inside Story. *The Sun Herald*, 2006, 8.
- [3] E. Bequerel. Recherches sur les effets de la radiation chimique de la lumière solaire, au moyen des courants électriques. *Comptes Rendus de L'Academie des Sciences*, 1839, 9, 145–149.
- [4] K. Tvrdy, P. A. Frantsuzov, and P. V. Kamat. Photoinduced Electron Transfer from Semiconductor Quantum Dots to Metal Oxide Nanoparticles. *The National Academy of Sciences*, 2011, 108, 29–34.
- [5] P. V. Kamat, K. Tvrdy, D. R. Baker, and J. G. Radich. Beyond Photovoltaics: Semiconductor Nanoarchitectures for Liquid Junction Solar Cells. *Chemical Reviews*, 2010, 110, 6664–6688.
- [6] D. M. Chapin, C. S. Fuller, and G. L. Pearson. A New Silicon p-n Junction Photocell for Converting Solar Radiation into Electrical Power. *Journal of Applied Physics*, 1954, 25(5), 676–677.
- [7] J. GERTNER. The Idea Factory: Bell Labs and the Great Age of American Innovation. *Penguin Books*, 2013.
- [8] W. A. Badawy, M.S. Morsi. Preparation and electrode properties of SnO<sub>2</sub> thin films *Bulletin of Electrochemistry*, 1989, 5, 276.
- [9] W. A. Badawy, Preparation and characterization of TiO<sub>2</sub>/Sb thin films for solar energy applications. *Solar Energy Materials and Solar Cells*, 1993, 28, 293.
- [10] A. Zaban, O. I. Mićić, B. A. Gregg and A. J. Nozik. Photosensitization of Nanoporous TiO<sub>2</sub> Electrodes with InP Quantum Dots. *Langmuir*, 1998, 14, 3153–3156.

- [11] A. J. Nozik. Quantum dot solar cells. *Physica E*, 2002, 14, 115–120.
- [12] P. V. Kamat. Quantum Dot Solar Cells. Semiconductor Nanocrystals as Light Harvesters. *The Journal of Physical Chemistry C*, 2008, 112, 18737–18753.
- [13] H. Lee, H. C. Leventis, S. J. Moon, P. Chen, S. Ito, S. A. Haque, T. Torres, F. Nüesch, T. Geiger, S. M. Zakeeruddin, M. Grätzel, and M. K. Nazeeruddin. PbS and CdS Quantum Dot-Sensitized Solid-State Solar Cells: “Old Concepts, New Results”. *Advanced Functional Materials*, 2009, 19, 2735–2742.
- [14] I. J. Kramer, E. H. Sargent. Colloidal quantum dot photovoltaics: a path forward. *ACS Nano*, 2011, 5, 8506–8514.
- [15] L. Yi, Y. Liu, N. Yang, Z. Tang, H. Zhao, G. Ma, Z. Sua and D. Wang. One dimensional CuInS<sub>2</sub>–ZnS heterostructured nanomaterials as low-cost and high-performance counter electrodes of dye-sensitized solar cells. *Energy & Environmental Science*, 2013, 6, 835–840.
- [16] H. Sun, J. He, J. Wang, S. Y. Zhang, C. Liu, T. Sritharan, S. Mhaisalkar, M. Y. Han, D. Wang and H. Chen. Investigating the Multiple Roles of Polyvinylpyrrolidone for a General Methodology of Oxide Encapsulation. *Journal of the American Chemical Society*, 2013, 135, 9099–9110.
- [17] N. Yang, Y. Liu, H. Wen, Z. Tang, H. Zhao, Y. Li and D. Wang. Photocatalytic Properties of Graphdiyne and Graphene Modified TiO<sub>2</sub>: From Theory to Experiment. *ACS Nano*, 2013, 7(2), 1504–1512.
- [18] L. Yi, D. Wang and M. Gao. Synthesis of Cu<sub>3</sub>SnS<sub>4</sub> nanocrystals and nanosheets by using Cu<sub>31</sub>S<sub>16</sub> as seeds. *CrystEngComm*, 2012, 14, 401–404.
- [19] Y. Cui, X. Lai, L. Li, Z. Hu, S. Wang, J. E. Halpert, R. Yu, D. Wang. Water-soluble monodispersed lanthanide oxide submicrospheres: PVP-assisted hydrothermal synthesis, size-control and luminescence properties. *ChemPhysChem*, 2012, 13, 2610.

- [20] A. L. Rogach, L. Katsikas, A. Kornowski, D. Su, A. Eychmüller, H. Weller, Ber. Bunsen. Synthesis and characterization of thiol-stabilized CdTe nanocrystals. *Berichte der Bunsen-Gesellschaft fur physikalische Chemie*, 1996, 100, 1772–1778.
- [21] L. E. Brus. Electron-electron and Electron-hole Interactions in Small Semiconductor Crystallites-the Size Dependence of the Lowest Excited Electronic State. *Journal of Chemical Physics*, 1984, 80, 4403–4409.
- [22] <http://www.sigmaaldrich.com/materials-science/nanomaterials/quantum-dots.html>.
- [23] [http://commons.wikimedia.org/wiki/File:Solar\\_Spectrum.png](http://commons.wikimedia.org/wiki/File:Solar_Spectrum.png).
- [24] B. Oregan, M. Gratzel. A low-cost, high-efficiency solar-cell based on dye-sensitized colloidal TiO<sub>2</sub> films. *Nature*, 1991, 353, 737–740.
- [25] Kevin Tvrdy. Electron transfer reaction in quantum dot sensitized solar cells. *University of Notre Dame*, 2011, 16–17.
- [26] Pokutnii SI. Exciton Binding Energy in Semiconductor Quantum Dots. *Semiconductors*, 2010, 44, 488–493.
- [27] Ramvall P, Tanaka S, Nomura S, Riblet P, Aoyagi Y. Observation of Confinement-Dependent Exciton Binding Energy of GaN Quantum Dots. *Applied Physics Letters*, 1998, 73, 1104–1106.
- [28] Nozik AJ. Spectroscopy and Hot Electron Relaxation Dynamics in Semiconductor Quantum Wells and Quantum Dots. *Annual Review of Physical Chemistry*, 2001, 52, 193–231.
- [29] Tisdale WA, et al. Hot-Electron Transfer from Semiconductor Nanocrystals. *Science*, 2010, 328, 1543–1547.
- [30] Schmidt K.H., MedeirosRibeiro G., Oestreich M., Petroff P.M., Dohler G.H. Carrier Relaxation and Electronic Structure in InAs Self-Assembled Quantum Dots. *Physical Review B: Condensed Matter*, 1996, 54, 11346–11353.

- [31] Grosse S, et al. Carrier Relaxation Dynamics in Quantum Dots: Scattering Mechanisms and State-Filling Effects. *Physical Review B: Condensed Matter*, 1997, 55, 4473–4476.
- [32] Eduardo Lorenzo. Solar Electricity: Engineering of Photovoltaic Systems. 1994, ISBN 84-86505-55-0.
- [33] Lindholm FA, Fossum JG, Burgess EL. Application of the superposition principle to solar-cell analysis. *IEEE Transactions on Electron Devices*, 1979, 26, 165–171.
- [34] Arturo Morales-Acevedo, Chapter 12, Solar Cells - Research and Application Perspectives, ISBN 978-953-51-1003-3.
- [35] J. A. Turner. A Realizable Renewable Energy Future. *Science*, 1999, 285 (5428), 687–689.
- [36] U. A. Joshi, A. Palasyuk, D. Arney, P. A. Maggard. Semiconducting Oxides to Facilitate the Conversion of Solar Energy to Chemical Fuels. *The Journal of Physical Chemistry Letters*, 2010, 1 (18), 2719–2726.
- [37] L. J. Minggu, W. R. Wan Daud, and M. B. Kassim. An overview of photocells and photoreactors for photoelectrochemical water splitting. *International Journal of Hydrogen Energy*, 2010, 35, 5233.
- [38] R. van de Krol, Y. Q. Liang, J. Schoonman. Solar Hydrogen Production with Nanostructured Metal Oxides. *Journal of Materials Chemistry*, 2008, 18, 2311–2320.
- [39] M. G. Walter, E. L. Warren, J. R. McKone, S. W. Boettcher, Q. X. Mi, E. A. Santori, N. S. Lewis. Solar Water Splitting Cells. *Chemical Reviews*, 2010, 110, 6446–6473.
- [40] H. Tong, S. Ouyang, Y. Bi, N. Umezawa, M. Oshikiri, and J. Ye. Nano-photocatalytic Materials: Possibilities and Challenges. *Advanced Materials*, 2012, 24, 229.

- [41] S. Choudhary, S. Upadhyay, P. Kumar, N. Singh, V. R. Satsangi, R. Shrivastav, and S. Dass. Nanostructured bilayered thin films in photoelectrochemical water splitting – A review. *International Journal of Hydrogen Energy*, 2012, 37, 18713.
- [42] A. Fujishima. Electrochemical Photolysis of Water at a Semiconductor Electrode. *Nature*, 1972, 238, 37–38.
- [43] X. L. Cui, M. Ma, W. Zhang, Y. H. Yang, Z. J. Zhang. Nitrogen-Doped TiO<sub>2</sub> from TiN and its Visible Light Photoelectrochemical properties. *Electrochemistry Communications*, 2008, 10, 367–371.
- [44] R. Ashai, T. Morokawa, T. Ohwaki, K. Aoki, Taga, Y. Visible-Light Photocatalysis in Nitrogen-Doped Titanium Oxides. *Science*, 2001, 293, 269–271.
- [45] K. Shankar, M. Paulose, G. K. Mor, O. K. Varghese, C. A. Grimes. A study on the spectral photoresponse and photoelectrochemical properties of flame-annealed titania nanotube-arrays. *Journal of Physics D: Applied Physics*, 2005, 38, 3543–3549.
- [46] S. Chen, M. Paulose, C. Ruan, G. K. Mor, O. K. Varghese, D. Kouzoudis, C. A. Grimes, Electrochemically synthesized CdS nanoparticle-modified TiO<sub>2</sub> nanotube-array photoelectrodes: Preparation, characterization, and application to photoelectrochemical cells. *Journal of Photochemistry and Photobiology A*, 2006, 177, 177–184.
- [47] J. Hensel, G. Wang, Y. Li and J. Z. Zhang. Synergistic Effect of CdSe Quantum Dot Sensitization and Nitrogen Doping of TiO<sub>2</sub> Nanostructures for Photoelectrochemical Solar Hydrogen Generation. *Nano letters*, 2010, 10, 478–483.
- [48] H. M. Chen, C. K. Chen, Y. C. Chang, C. W. Tsai, R. S. Liu, S. F. Hu, W. S. Chang and K. H. Chen. Quantum Dot Monolayer Sensitized ZnO Nanowire-Array Photoelectrodes: True Efficiency for Water Splitting. *Angewandte Chemie*, 2010, 49, 5966–5969.

- [49] H. Kim, M. Seol, J. Lee and K. Yong. Highly Efficient Photoelectrochemical Hydrogen Generation Using Hierarchical ZnO/WO<sub>x</sub> Nanowires Cosensitized with CdSe/CdS. *The Journal of Physical Chemistry C*, 2011, 115, 25429–25436.
- [50] J. Luo, S. K. Karuturi, L. Liu, L. T. Su, A. I. Tok and H. J. Fan. Homogeneous Photosensitization of Complex TiO<sub>2</sub> Nanostructures for Efficient Solar Energy Conversion. *Scientific reports*, 2012, 2, 451.
- [51] J. M. Luther, M. Law, M. C. Beard, Q. Song, M. O. Reese, R. J. Ellingson, A. J. Nozik. Schottky Solar Cells Based on Colloidal Nanocrystal Films. *Nano Letters*, 2008, 8, 3488–3492.
- [52] R. Debnath, J. Tang, D. A. Barkhouse, X. Wang, A. G. Pattantyus-Abraham, L. Brzozowski, L. Levina, E. H. Sargent. Ambient-Processed Colloidal Quantum Dot Solar Cells via Individual Pre-Encapsulation of Nanoparticles. *Journal of the American Chemical Society*, 2010, 132, 5952–5953.
- [53] A. Braga, S. Giménez, I. Concina, A. Vomiero, and I. Mora-Seró. Panchromatic Sensitized Solar Cells Based on Metal Sulfide Quantum Dots Grown Directly on Nanostructured TiO<sub>2</sub> Electrodes. *The Journal of Physical Chemistry Letters*, 2011, 2 (5), 454–460.
- [54] Y. L. Lee, B. M. Huang, H. T. Chien. Highly Efficient CdSe-Sensitized TiO<sub>2</sub> Photoelectrode for Quantum-Dot-Sensitized Solar Cell Applications. *Chemistry of Materials*, 2008, 20, 6903–6905.
- [55] O. Niitsoo, S. K. Sarkar, C. Pejoux, S. Ruhle, D. Cahen, G. Hodes. Chemical Bath Deposited CdS/CdSe-Sensitized Porous TiO<sub>2</sub> Solar Cells. *Journal of Photochemistry and Photobiology A*, 2006, 181, 306–313.
- [56] A. G. Pattantyus-Abraham, I. J. Kramer, A. R. Barkhouse, X. Wang, G. Konstantatos, R. Debnath, L. Levina, I. Raabe, M. K. Nazeeruddin, M. Gratzel, E. H.

Sargent. Depleted-Heterojunction Colloidal Quantum Dot Solar Cells. *ACS Nano* 2010, 4, 3374–3380.

- [57] L. J. Diguna, Q. Shen, J. Kobayashi and T. Toyoda. High efficiency of CdSe quantum-dot-sensitized TiO<sub>2</sub> inverse opal solar cells. *Applied Physics Letters*, 2007, 91, 023116.
- [58] I. Mora- Seró, S. Gimenez, F. Fabregat-Santiago, R. Gomez, Q. Shen, T. Toyoda and J. Bisquert. Recombination in quantum dot sensitized solar cells. *Accounts of Chemical Research*, 2009, 42, 1848–1857.
- [59] S. Hachiya, Q. Shen and T. Toyoda. Effect of ZnS coatings on the enhancement of the photovoltaic properties of PbS quantum dot-sensitized solar cells. *Journal of Applied Physics*, 2012, 111, 104315.
- [60] S. S. Mali, S. K. Desai, S. S. Kalagi, C. A. Betty, P. N. Bhosale, R. S. Devan, Y. R. Ma and P. S. Patil. PbS quantum dot sensitized anatase TiO<sub>2</sub> nanocorals for quantum dot-sensitized solar cell applications. *Dalton Transactions*, 2012, 41, 6130–6136.
- [61] D. R. Baker and P. V. Kamat. Photosensitization of TiO<sub>2</sub> Nanostructures with CdS Quantum Dots: Particulate versus Tubular Support Architectures. *Advanced Functional Materials*, 2009, 19, 805–811.
- [62] S. Giménez, I. Mora-Seró, L. Macor, N. Guijarro, T. Lana-Villarreal, R. Gómez, L. J. Diguna, Q. Shen, T. Toyoda, J. Bisquert. Improving the performance of colloidal quantum-dot-sensitized solar cells. *Nanotechnology*, 2009, 20, 295204.
- [63] A. Salant, M. Shalom, I. Hod, A. Faust, A. Zaban, U. Banin. Quantum Dot Sensitized Solar Cells with Improved Efficiency Prepared Using Electrophoretic Deposition. *ACS Nano*, 2010, 4, 5962–5968.

- [64] I. Robel, V. Subramanian, M. Kuno, P. V. Kamat. Quantum Dot Solar Cells. Harvesting Light Energy with CdSe Nanocrystals Molecularly Linked to Mesoscopic TiO<sub>2</sub> Films. *Journal of the American Chemical Society*, 2006, 128, 2385–2393.
- [65] Z. Pan, H. Zhang, K. Cheng, Y. Hou, J. Hua and X. Zhong. Highly Efficient Inverted Type-I CdS/CdSe Core/Shell Structure QD-Sensitized Solar Cells. *ACS Nano*, 2012, 6, 3982.
- [66] I. Mora-Seró, S. Gimenez, T. Moehl, F. Fabregat-Santiago, T. Lana-Villareal, R. Gomez, J. Bisquert. Factors Determining the Photovoltaic Performance of a CdSe Quantum Dot Sensitized Solar Cell: The Role of the Linker Molecule and of the Counter Electrode. *Nanotechnology*, 2008, 19, 424007.
- [67] N. Guijarro, T. Lana-Villarreal, I. Mora-Sero, J. Bisquert, R. Gomez. CdSe Quantum Dot-Sensitized TiO<sub>2</sub> Electrodes: Effect of Quantum Dot Coverage and Mode of Attachment. *The Journal of Physical Chemistry C*, 2009, 113, 4208–4214.
- [68] P. Sarkar, P. S. Nicholson. Electrophoretic Deposition (EPD): Mechanisms, Kinetics, and Application to Ceramics. *Journal of the American Ceramic Society*, 1996, 79, 1987–2002.
- [69] A. R. Boccaccini, J. A. Roether, B. J. C. Thomas, M. S. P. Shaffer, E. Chavez, E. Stoll, E. J. Minay. The electrophoretic deposition of inorganic nanoscaled materials : A review. *Journal of the Ceramic Society of Japan*, 2006, 114 (1), 1–14.
- [70] M. E. Wong, P. C. Searson. ZnO Quantum Particle Thin Films Fabricated by Electrophoretic Deposition. *Applied Physics Letters*, 1999, 74, 2939–2941.
- [71] S. V. Mahajan, J. Cho, M. S. P. Shaffer, A. R. Boccaccini, J. H. Dickerson. Electrophoretic deposition and characterization of Eu<sub>2</sub>O<sub>3</sub> nanocrystal—Carbon nanotube heterostructures. *Journal of the European Ceramic Society*, 2010, 30, 1145–1150.

- [72] M.Giersig, P. Mulvaney. Formation of Ordered Two-Dimensional Gold Colloid Lattices by Electrophoretic Deposition. *The Journal of Physical Chemistry*, 1993, 97, 6334–6336.
- [73] M. N. Patel, R. D. Williams, R. A. May, H. Uchida, K. J. Stevenson, K. P. Johnston. Electrophoretic Deposition of Au Nanocrystals inside Perpendicular Mesochannels of TiO<sub>2</sub>. *Chemistry of Materials*, 2008, 20, 6029–6040.
- [74] L. Grinis, S. Dor, A. Ofir, A. Zaban. Electrophoretic Deposition and Compression of Titania Nanoparticle Films for Dye-Sensitized Solar Cells. *Journal of Photochemistry and Photobiology A*, 2008, 198, 52–59.
- [75] B. Ferrari, A. Bartret, C. Baudin. Sandwich materials formed by thick alumina tapes and thin-layered alumina–aluminium titanate structures shaped by EPD. *Journal of the European Ceramic Society*, 2009, 29, 1083–1092
- [76] M. Vidotti, S. I. C. de Torresi, Electrostatic Layer-by-Layer and Electrophoretic Depositions as Methods for Electrochromic Nanoparticle Immobilization. *Electrochim. Acta*, 2009, 54, 2800–2804.
- [77] N. J. Smith, K. J. Emmett and S. J. Rosenthal. Photovoltaic cells fabricated by electrophoretic deposition of CdSe nanocrystals. *Applied Physics Letters*, 2008, 93, 043504.
- [78] N. P. Benehkohal, V. González-Pedro, P. P. Boix, S. Chavhan, R. Tena-Zaera, G. P. Demopoulos and I. Mora-Seró. Colloidal PbS and PbSeS Quantum Dot Sensitized Solar Cells Prepared by Electrophoretic Deposition. *The Journal of Physical Chemistry C*, 2012, 116 (31), 16391–16397.
- [79] I. Hod, V. González-Pedro, Z. Tachan, F. Fabregat-Santiago, I. Mora-Seró, J. Bisquert; A. Zaban, Dye versus Quantum Dots in Sensitized Solar Cells: Participation of Quantum Dot Absorber in the Recombination Process. *The Journal of Physical Chemistry Letters*, 2011, 2 (24), 3032–3035.

- [80] K. Szendrei, M. Speirs, W. Gomulya, D. Jarzab, M. Manca, O. V. Mikhnenko, M. Yarema, B. J. Kooi, W. Heiss and M. A. Loi. Exploring the Origin of the Temperature-Dependent Behavior of PbS Nanocrystal Thin Films and Solar Cells. *Advanced Functional Materials*, 2012, 22, 1598–1605.
- [81] J. Tang, K. W. Kemp, S. Hoogland, K. S. Jeong, H. Liu, L. Levina, M. Furukawa, X. H. Wang, R. Debnath, D. K. Cha, K. W. Chou, A. Fischer, A. Amassian, J. B. Asbury, E. H. Sargent. Colloidal-quantum-dot photovoltaics using atomic-ligand passivation. *Nature Materials*, 2011, 10 (10), 765–771.
- [82] B. O. Dabbousi, J. Rodriguez-Viejo, F. V. Mikulec, J. R. Heine, H. Mattoussi, R. Ober, K. F. Jensen and M. G. Bawendi. (CdSe) ZnS core-shell quantum dots: Synthesis and characterization of a size series of highly luminescent nanocrystallites. *Journal of Physical Chemistry B*, 1997, 101 (46), 9463–9475.
- [83] L. Dworak, V. V. Matylitsky, V. V. Breus, M. Braun, T. Basche, J. Wachtveitl. Ultrafast Charge Separation at the CdSe/CdS Core/Shell Quantum Dot/Methylviologen Interface: Implications for Nanocrystal Solar Cells. *Journal of Physical Chemistry C*, 2011, 115 (10), 3949–3955.
- [84] H. Zhao, T. Zhang, M. Chaker, and D. Ma. Ligand and Precursor Effects on the Synthesis and Optical Properties of PbS Quantum Dots. *Journal of Nanoscience and Nanotechnology*, 2010, 10, 4897–4905.
- [85] M. Pietryga, D. J. Werder, D. J. Williams, J. L. Casson, R. D. Schaller, V. I. Klimov, and J. A. Hollingsworth. Utilizing the Lability of Lead Selenide to Produce Heterostructured Nanocrystals with Bright, Stable Infrared Emission. *Journal of the American Chemical Society*, 2008, 130, 4879–4885.
- [86] H. Zhao, M. Chaker, and D. Ma. Effect of CdS Shell Thickness on the Optical Properties of Water-soluble Amphiphilic Polymer Encapsulated PbS/CdS Quantum

Dots. *Journal of Materials Chemistry, Journal of Materials Chemistry*, 2011, 21, 17483–17491.

- [87] H. G. Zhao, M. Chaker, N. Q. Wu, D. L. Ma. Towards controlled synthesis and better understanding of highly luminescent PbS/CdS core/shell quantum dots. *Journal of Materials Chemistry*, 2011, 21 (24), 8898–8904.
- [88] H. Zhao , Z. Fan , H. Liang , G. S. Selopal , B. A. Gonfa , L. Jin , A. Soudi , D. Cui , F. Enrichi , M. M. Natile , I. Concina , D. Ma , A. O. Govorov , F. Rosei and A. Vomiero. Controlling photoinduced electron transfer from PbS@CdS core@shell quantum dots to metal oxide nanostructured thin films. *Nanoscale*, 2014, 6, 7004–7011.
- [89] T. Zhang, H. G. Zhao, D. Riabinina, M. Chaker, D. L. Ma. Concentration-Dependent Photoinduced Photoluminescence Enhancement in Colloidal PbS Quantum Dot Solution. *Journal of Physical Chemistry C*, 2010, 114 (22), 10153–10159.
- [90] H. G. Zhao. Synthesis and Characterization of High-quality Near Infrared-emitting Quantum Dots in an Organic Phase or in Water Université du Québec INRS-EMT. 2011, 15.
- [91] H. G. Zhao, D. F. Wang, T. Zhang, M. Chaker, D. Ma. Two-step Approach to Synthesize Water-soluble Near-infrared Emitting Colloidal Quantum Dots via Amphiphilic Polymers. *Chemical Communications*, 2010, 46 (29), 5301–5303.
- [92] M. A. Islam, Y. Q. Xia, D. A. Telesca, M. L. Steigerwald, I. P. Herman. Controlled Electrophoretic Deposition of Smooth and Robust Films of CdSe Nanocrystals. *Chemistry of Materials*, 2004, 16, 49–54.
- [93] R. Krishnan, M. A. Hahn, Z. Yu, J. Silcox, P. M. Fauchet, T. D. Krauss. Polarization Surface-Charge Density of Single Semiconductor Quantum Rods. *Physical Review Letters*, 2004, 92 (21), 216803 (1)–216803 (4).

- [94] G. Kalyuzhny, R. W. Murray. Ligand Effects on Optical Properties of CdSe Nanocrystals. *The Journal of Physical Chemistry B*, 2005, 109, 7012–7021.
- [95] H. Mehrer. Analysis and Simulation of Semiconductor Devices, 2007, ISSN 0171–1873, ISBN 978-3-540-71486-6.
- [96] L. Kavan, M. Gratzel, Highly Efficient Semiconducting TiO<sub>2</sub> Photoelectrodes Prepared by Aerosol Pyrolysis. *Electrochimica Acta* 1995, 40, 643–652.
- [97] L. Jin, H. Zhao, D. Ma, A. Vomiero, and F. Rosei. Dynamics of semiconducting nanocrystal uptake into mesoporous TiO<sub>2</sub> thick films by electrophoretic deposition. *Journal of Materials Chemistry A*, 2015, 3, 847.
- [98] Y.-L. Lee and C.-H. Chang. Efficient polysulfide electrolyte for CdS quantum dot-sensitized solar cells. *Journal of Power Sources*, 2008, 185 (1), 584–588.
- [99] R. Trevisan, P. Rodenas, V. Gonzalez-Pedro, C. Sima, R. S. Sanchez, E. M. Barea, I. Mora-Sero, F. Fabregat-Santiago and S. Gimenez. Harnessing infrared photons for photoelectrochemical hydrogen generation. A PbS quantum dot based “quasi-artificial leaf”. *The Journal of Physical Chemistry Letters*, 2013, 4, 141–146.
- [100] M. G. Debije and P. P. C. Verbunt, Thirty years of luminescent solar concentrator research: solar energy for the built environment. *Advanced Energy Materials*, 2012, 2, 12–35.
- [101] J. Yoon, L. Li, A. V. Semichaevsky, J. H. Ryu, H. T. Johnson, R. G. Nuzzo and J. A. Rogers, Flexible Concentrator Photovoltaics Based on Microscale Silicon Solar Cells Embedded in Luminescent Waveguides. *Nature communications*, 2011, 2, 343.
- [102] W. G. van Sark, K. W. Barnham, L. H. Slooff, A. J. Chatten, A. Büchtemann, A. Meyer, S. J. McCormack, R. Koole, D. J. Farrell and R. Bose. Luminescent Solar Concentrators-A review of recent results. *Optics Express*, 2008, 16, 21773–21792.

[ 103 ] S. Licht. Solar water splitting to generate hydrogen fuel: photothermal electrochemical analysis. *The Journal of Physical Chemistry B*, 2003, 107, 4253–4260.

[104] S. Licht, L. Halperin, M. Kalina, M. Zidman and N. Halperin, Electrochemical Potential Tuned Solar Water Splitting. *Chemical Communications*, 2003, 3006–3007.

[105] Principles of Semiconductor Devices online textbook by Van Zeghbroeck, Chapter 2.7

## APPENDIX RESUME

### 1. INTRODUCTION

La lutte contre le changement climatique est le plus gros challenge du XXI<sup>e</sup> siècle [1]. Afin de limiter l'augmentation des émissions de gaz à effet de serre, des sources d'énergie alternatives au charbon, au pétrole et au gaz doivent être proposées. L'une de ces alternatives, celle qui est de loin la plus abondante est l'énergie solaire. Cette dernière représente dix-mille fois l'énergie journalière consommée par l'humanité [2]. Cependant ce ne fut qu'en 1839 que le physicien français A. E. Becquerel découvrit l'effet photovoltaïque, marquant l'émergence de l'utilisation humaine des radiations solaires [3]. La compréhension de la nature fondamentale de ce phénomène par Albert Einstein [4] a ouvert la voie aux laboratoires Bell pour développer les cellules photovoltaïques (PV) en silicium [5], les premières cellules solaires capables de produire suffisamment d'énergie pour alimenter un équipement électronique. Cependant, à cause des coûts de production, de la pénurie de gaufre de silicium, et des limitations inhérentes au matériau silicium, des progrès en terme de R&D des nouvelles cellules photovoltaïques sont nécessaires afin de réduire le prix et d'augmenter le rendement.

Ces dernières années, les nanocristaux semi-conducteurs (Quantum Dot's SemiConductors, QDSC), aussi appelés "quantum dots (QD)" ont attiré l'attention de la communauté scientifique en raison de leur spectre d'absorption ajustable [6]. Plus spécifiquement, plus le confinement est fort, c'est à dire plus la taille du point quantique est petit, plus la bande interdite (bandgap) du matériau est large (Figure 1.1 (b)), comme décrit par l'équation [7] ci-dessous.

$$E = E_g + (\hbar^2 \pi^2 / 2R^2) (1/m_e + 1/m_h) - 1.8e^2 / \epsilon R \quad \text{Équation 1.1}$$

Où  $E_g$  est l'énergie de la bande interdite du matériau massif correspondant,  $\hbar$  est la constante de Plank,  $m_e$  et  $m_h$  sont, respectivement, la masse effective des électrons et des trous,  $e$  est la charge de l'électron,  $R$  le rayon, et  $\epsilon$  la constante diélectrique du QD.

Afin d'atteindre une efficacité maximale, il faut convertir chaque région du spectre solaire efficacement en changeant l'épaisseur de la bande interdite du matériau (Figure 1.1 (c)), ce qui veut dire, pour les QD, de changer la taille des cristaux. Ainsi des QD sont introduits dans des cellules solaires en tant que catalyseur optique [8, 9, 10, 11]. En particulier, les QD qui sont actifs dans le domaine optique du proche infrarouge tels que PbS [12] et PbSe [13] ont attiré énormément d'intérêt comme catalyseur optique parce qu'ils permettent d'étendre la bande d'absorption vers la partie proche infrarouge du spectre.

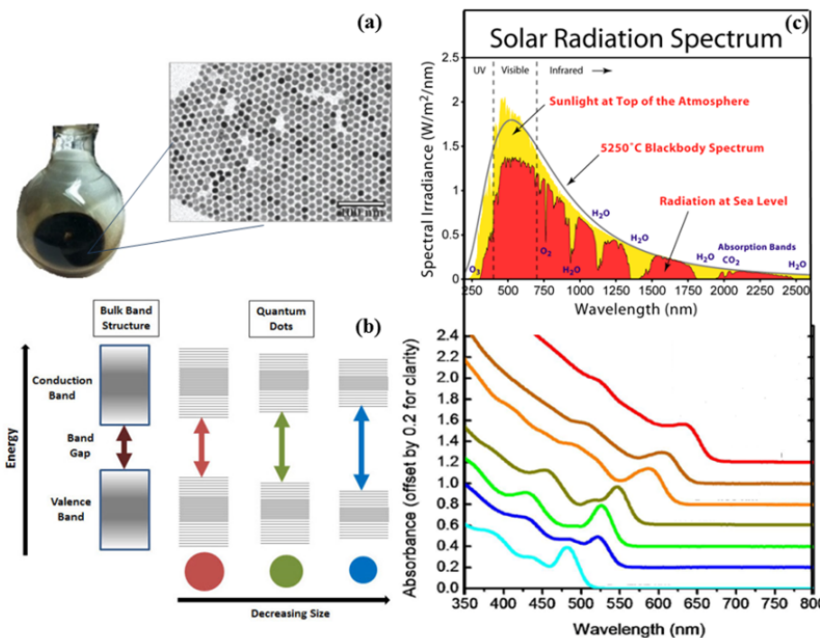


**Figure 1.1** Image montrant (a) des quantum dots de PbS colloïdaux. Encart : Image en Microscopie électronique en transmission (TEM) avec une résolution de 1.5 nm (b) diagramme énergétique des quantum dots dû à l'effet de confinement quantique, la bande d'exclusion des semi-conducteurs augmente quand la taille du nanocrystal diminue. [14] (c) Spectre solaire et spectre d'absorption réglable ajusté par les QD correspondant. [15]

Dans une configuration spéciale de QDSC [16] (Figure 1.2 (a)), les QD sont greffés sur la surface d'un semi-conducteur ayant une bande d'exclusion large [17, 18]. Comme le diagramme d'énergie le montre sur la Figure 1.2 (b), les QD absorbent la lumière et un exciton est créé. Ensuite, l'exciton se dissocie à l'interface QD/Oxyde, et l'électron est injecté dans l'oxyde qui sert de transporteur à l'électron [19]. Un électrolyte liquide complète le système électrochimique en permettant la neutralisation du QD après

l'injection électronique. C'est pour cela que l'un des challenges importants est de concevoir un procédé abordable d'incorporer des QD sur l'oxyde et d'arriver efficacement à une jonction QD - électrode qui promouvrait la séparation de charge, tout en minimisant la capture des charges en surface et les pertes des charges. Des méthodes de croissance *in situ* ont été couramment utilisées malgré le fait qu'elles ne permettent pas de contrôler indépendamment la taille et la répartition des QD [11]. Ces inconvénients peuvent être évités si les QD sont synthétisés avant la catalyse optique sous forme de colloïdes, puis sont greffés en surface de l'oxyde. La déposition électrophorétique (EPD), une technique couramment utilisée, est basée sur la notion de greffage de particules chargées sous un champ électrique. Cette méthode présente de nombreux avantages par rapport à d'autres techniques. En particulier cette méthode est économique, ne demande pas trop de temps de procédé, ne demande pas d'équipements complexes et résulte en la formation d'une couche de QD d'épaisseur contrôlée [20, 21]. L'EPD a déjà été utilisé pour déposer des nanoparticules semi-conductrices [22, 23], métalliques [24, 25] ou isolantes [26, 27] sur des substrats conducteurs ou des films polymères [25, 28]. La première utilisation dans le domaine des cellules photovoltaïques de l'EPD publiée fut pour la déposition de nanoparticules. [26] Les QD en sélénure de cadmium colloïdal déposé par EPD sur film mince a été utilisé comme démonstrateur technique pour application photovoltaïques, le rendement PCEs est bas ( $10^{-6}$  %) dû à la faible densité optique de la cellule photovoltaïque [29]. Afin d'augmenter la surface efficace active, les QD de CdSe ont été incorporés dans des couches de TiO<sub>2</sub> poreux de plusieurs microns d'épaisseur [30], ce qui permis d'atteindre une efficacité pouvant atteindre jusqu'à 1,7 % sous une unité d'illumination solaire. L'équipe de Mora-Seró [31] a préparé des QDSC par déposition de QD de PbS et PbSe colloïdaux sur des films de TiO<sub>2</sub> mésoporeux par EPD. Les paramètres de taille et de temps d'EPD ont démontré une forte influence sur les performances, ce qui permet d'identifier les facteurs clés pour le développement efficace des QDSC. De plus, la diminution de la résistance de recombinaison avec le temps d'EPD prouve indubitablement que la couverture du TiO<sub>2</sub> par les QD réduirait la recombinaison des charges depuis le TiO<sub>2</sub> vers les électrolytes. [32] C'est pour cela qu'un contrôle adéquat des paramètres déterminant l'absorption des QD et la couverture des oxydes est

obligatoire. Néanmoins, pour l'instant, seulement des démonstrations génériques d'une pénétration quasiment constante des QD dans les films est démontrée, et ce basé sur des analyses de spectres X de basse résolution (spectroscopie X EDX), [29] et aucune analyse systématique de l'absorption des QD n'est présente dans la littérature.

D'autre part, l'autre défi de ce type de cellules photovoltaïques est le développement de QDSC stable sur de longues durées. En fait, les QD, à cause de leur grand ratio surface sur volume, sont très sensibles aux défauts de surface et à l'oxydation, ce qui cause des recombinaisons [33] menant à une baisse de l'efficacité de photoconversion (PhotoConvesion Efficiency PCE). [34] C'est pour cela que les QD étaient habituellement encapsulés dans des ligands organiques [35, 36] alors que les liaisons ballantes restant sur la surface des QD peuvent se comporter en site de recombinaisons si la dépassivatlon partielle des ligands à lieu [37]. Des études récentes [38, 39, 40] ont révélé qu'une coque inorganique robuste, de bande plus large, peut permettre de passiver de manière plus efficace la surface des QD, contribuant à une stabilité chimique, thermique et photochimique largement améliorée, mais aussi un taux d'injection des charges dans les QD acceptables pour une taille de noyau et une épaisseur de croute optimale [41].

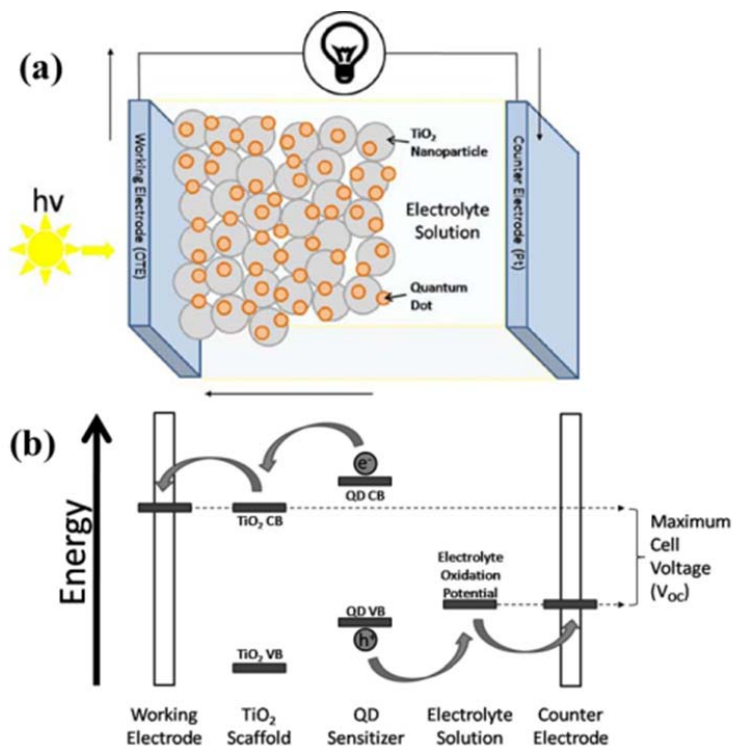


**Figure 1.2** Image artistique de (a) les matériaux composant la cellule solaire à base d'un quantum dot et d'un catalyseur optique. Les flèches noires autour de la cellule matérialisent la direction du flux d'électrons (b) le diagramme énergétique à la base de la mise en mouvement des électrons et des trous dans la cellule solaire à base d'un quantum dot et d'un catalyseur optique. [42]

## Objectifs

Afin de trouver une réponse à ces limitations et d'étudier les QDSC en profondeur, je compte synthétiser et étudier les photoanodes en couplant des QD de PbS ou de PbS@CdS sur des films de TiO<sub>2</sub>. Les objectifs du projet en découlant sont les suivants :

- 1) Déposition de QD de *ex-situ* PbS ou PbS@CdS externes dans des films de TiO<sub>2</sub> par méthode EPD et étude de la stabilité des QD après EPD.
- 2) une étude systématique de la dynamique des QD proche infrarouge chargés dans les films de dioxyde de titane par EPD.
- 3) Une étude de la tension et du temps d'EPD sur l'absorption des QD en utilisant des QD noyau@coquille de PbS@CdS en tant que capteur solaire hautement stable.

## 2. EXPÉRIENCES

Dans ce chapitre je parlerai premièrement de la synthèse des QD de PbS colloïdaux de 3.0 nm de diamètre via une méthode d'injection à chaud en utilisant OA comme liguant. [43] Puis des QD de PbS@CdS ont été synthétisés à l'aide d'une méthode d'échange de cation [39], avec des épaisseurs de coquille de 0,2 - 0,5 nm en variant la taille des nanoparticules de PbS utilisées pour le cœur ainsi que d'autres paramètres réactionnels tels le ratio entre le Pb et le Cd et le temps de réaction. Tous les QD étaient en "dispersion" dans du toluène. Le film de dioxyde de titane était déposé sur le FTO par coulage en bande et fritté à 450° pendant 30 minutes, formant un film transparent de 6 $\mu$ m d'épaisseur. Pendant le processus d'EPD, une paire de bandes de FTO couverte de TiO<sub>2</sub> ont été immergées verticalement dans une solution de QD face à face (Figure 2.1 (a)). La distance entre les deux bandes a été réglée à 1 cm et la surface de déposition des électrodes était d'environ 0.72 cm<sup>2</sup>. Un Voltage de 50 V à 200 V a été appliqué pour une durée de 5 - 120 min. Afin de nettoyer les QD qui ne seraient pas liés à la surface après la cataphorèse, les échantillons ont été rincés plusieurs fois par du toluène et séchées sous azote à température ambiante.

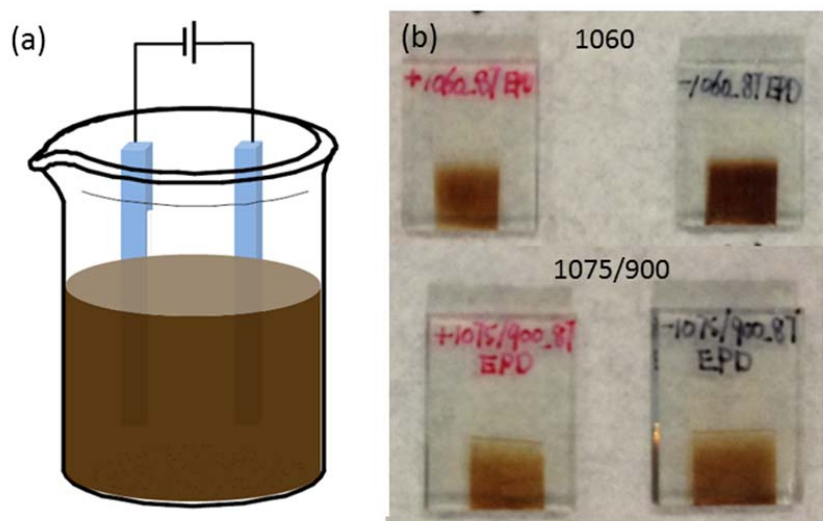


Figure 2.1 (a) description du système de déposition EPD; (b) Photographies des électrodes de TiO<sub>2</sub> après EPD des QD pendant une heure.

Puis je présente la méthode de caractérisation des échantillons. Nous avons utilisé des microscopes électroniques à balayage (Scanning Electron Microscopy, SEM) afin

d'étudier la morphologie des échantillons et un microscope électronique en transmission (Transmission Electrons Microscopy, TEM) afin d'obtenir la distribution des QD sur la surface de TiO<sub>2</sub> après EPD. La sensibilité de la condition de déposition des QD nous pousse à nous concentrer sur la stabilité des QD après EPD. La stabilité structurelle a été étudiée par XPS, par lequel nous pouvons obtenir des informations sur les liaisons chimiques et leur évolution dans le temps. La stabilité des propriétés optiques (l'absorbance et la Photoluminescence, PL) a été testée quantitativement par PL, ce qui est particulièrement sensible à la taille du noyau de PbS. La rétrodiffusion Rutherford (Rutherford Backscattering, RBS) a été utilisée pour déterminer la composition et l'épaisseur des QD dans le film mésoporeux.

### **3. DYNAMIQUE DE L'ABSORPTION DES QD DANS DES FILMS ÉPAIS DE TiO<sub>2</sub> MÉSOPOREUX PAR EPD**

Dans ce chapitre, je discute de la caractérisation des QD en solution et dans le film de TiO<sub>2</sub> après l'EPD. Le spectre d'absorption des échantillons avec différentes tailles de QD de PbS et de PbS@CdS en solution dans le toluène a été utilisé afin de déterminer le diamètre moyen des PbS [44]. L'épaisseur de la coquille de CdS dans les QD de PbS@CdS peut être obtenue par simple soustraction entre la taille totale du QD telle que mesurée par TEM et la taille du noyau de PbS [44]. La Croute des QD de PbS@CdS est principalement composée de CdS. Le diamètre total du QD (dtotal), diamètre du noyau (dcore), l'épaisseur de la croute (dshell), la position du premier pic d'absorption exitronique et de PL sont listés dans la table.

**Tableau 3.1 Dimension et propriétés optiques de QD pures et enrobées considérées dans cette étude. La taille moyenne des PbS@CdS est basée sur l'observation TEM, la taille du noyau est estimée avec la position du premier pic exitronique et l'épaisseur de la croute est estimée par soustraction**

Sample	Diameter (nm)	Core Diameter (nm)	Shell thickness (nm)	Abs max (nm)	PL max (nm)
PbS_S	3.09±0.3	3.09	0	912	
PbS_M	3.69±0.3	3.69	0	1079	
PbS_L	4.11±0.3	4.07	0	1184	
PbS@CdS_S	3.12±0.3	2.98	0.07	879	920
PbS@CdS_M	3.68±0.3	3.26	0.21	961	1075
PbS@CdS_L	4.10±0.3	3.44	0.33	1012	1180

Les QD ainsi synthétisés ont été déposés sur des couches de TiO<sub>2</sub> mésoporeux par EPD. L'épaisseur du film de TiO<sub>2</sub> était d'environ 6 µm, tel qu'estimé par profilomètre et vue en coupe par SEM. Après EPD des QD, les électrodes chargées positivement et négativement ont été colorées, de manière cohérente avec les études précédentes [30, 31], indiquant la déposition de QD chargés positivement et négativement. Cet effet peut être compris comme une perte de ligands préférentielle [45, 46, 47]. La déposition efficace des QD sur le TiO<sub>2</sub> est validée par l'EDX en SEM, dans lequel les signaux dus au Cd, au Pb et au S sont clairement visibles. Les Images TEM des électrodes de TiO<sub>2</sub> catalysés optiquement par des QD cœur@gaine de PbS@CdS pour différents temps d'EPD indiquent que le processus d'EPD produit des couvertures de QD qui augmentent en densité lorsqu'on augmente le temps de déposition et qui sont bien définis spatialement. Il n'y a pas de signes évidents d'agrégation des QD, ce qui serait problématique pour le transfert d'électrons dans le dispositif.

Afin de vérifier l'effet de l'EPD sur la stabilité structurelle et sur les propriétés optiques des QD, nous avons effectué des analyses XPS et PL des QD déposés sur des surfaces de Silicium ou après EPD sur des surfaces de films de TiO<sub>2</sub> mésoporeux. Nous avons comparé les QD avec et sans gangue de CdS afin de tester la capacité de cette gangue à prévenir la dégradation des QD. L'XPS a été utilisé pour caractériser les effets de l'EPD sur les liaisons chimiques dans les QD, cela nous a montré l'augmentation des dommages dans les QD de PbS pur, alors que, les structures cœur@gaine, il n'y a pas d'indice de création de liaisons pendantes, et une stabilité structurale meilleure. Les spectres de PL démontrent clairement l'augmentation de stabilité optique du à la présence de la gaine de passivation.

L'augmentation de la stabilité des QD cœur@gaine nous a motivé à sélectionner cette structure pour investiguer la dynamique d'absorption des QD pendant l'EPD en utilisant le RBS. Nous nous sommes concentrés sur la mesure du profil en profondeur du Pb, sous l'hypothèse raisonnable que la structure cœur@gaine et le ratio atomique de Pb/Cd est préservé après EPD et que donc, en principe, le profil en épaisseur du Cd est le même que celui du Pb. Dans la Figure 3.1, deux régions différentes régions peuvent être clairement identifiées : dans la région A, la concentration en Pb est quasiment constante et ne dépend pas de la profondeur, et augmente exponentiellement avec le temps d'EPD ; dans la région B, un pic de concentration en surface de Pb se forme après 5 minutes de déposition EPD, et la concentration de surface augmente en fonction du temps jusqu'à un seuil de saturation.

Nous calculons le paramètre principal du Pb en fonction du temps d'EPD à l'aide d'un spectre RBS : (i) La concentration atomique du Pb en surface (pic de surface dans la région B) ; (ii) Concentration atomique du Pb à l'interface avec le FTO (région A) (iii) La profondeur de pénétration du Pb. Avec  $C(x,t)$  la concentration atomique du Pb en fonction de la position dans le film et  $t$  la durée d'EPD, et  $C_s(t)$  et  $C_i(t)$  étant la concentration atomique en Pb respectivement à la surface du film et à l'interface FTO/TiO<sub>2</sub>,  $x_0$  étant définis comme suit :

$$C(x_0, t) - C_i(t) = \frac{C_s(t) - C_i(t)}{2} \quad \text{Équation 3.1}$$

Une définition empirique de la concentration en Pb en fonction du temps d'EPD et de la position dans le film en prenant pour hypothèse que le processus d'absorption des QD en début d'EPD et le processus de diffusion des QD (diffusion de Fick) due à l'augmentation du gradient de concentration en QD sont mutuellement indépendants.

Sous ces hypothèses, la concentration  $C(x,t)$  peut être écrite comme suis :

$$C(x,t) = C_0 \left[ 1 - \exp\left(-\frac{t}{\tau}\right) \right] + C_1 \left[ 1 - \operatorname{erf}\left(\frac{x}{2\sqrt{Dt}}\right) \right] \quad \text{Équation 3.2}$$

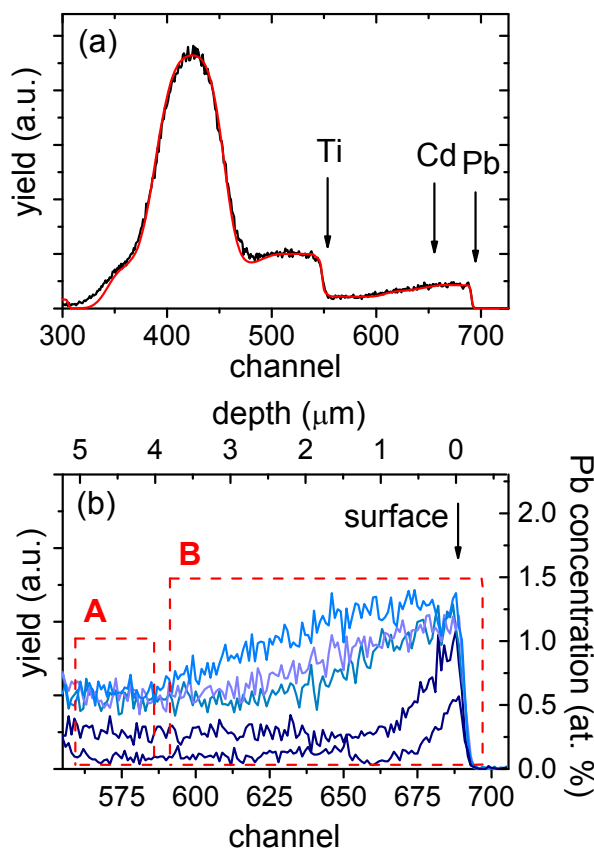


**Figure 3.1** (a) Spectre RBS du film de Titane mésoporeux catalysé optiquement avec des QD durant 120 minutes. La courbe rouge est le résultat d'une simulation avec le code RUMP. Le bord des surfaces du Ti, Cd et Pb est indiqué par des flèches. (b) signal RBS des régions spectrales présentant un signal du Pb pour des échantillons catalysés optiquement durant différentes durées (5, 10, 30, 60 ,120 minutes, du bleu sombre au bleu le plus clair). Les rectangles A et B soulignent deux régions dans laquelle la diffusion des QD ne peut être détectée (A) ou est clairement visible (B).

Lors de l'interpolation  $C_0$ ,  $C_1$  et D sont déterminés expérimentalement.  $C_0$  est la concentration asymptotique du Pb dans la région A après 120 minutes d'EPD, et est calculée à partir de la concentration atomique en Pb dans la région A en fonction du temps,  $C_1$  est la concentration asymptotique à la surface du film de  $\text{TiO}_2$ , et D est le coefficient de diffusion calculé à l'aide d'un fit linéaire de la variation du paramètre  $x_0$  en fonction de la racine carrée du temps d'EPD.

Une reconstruction du profil de concentration du Pb en fonction du temps d'EPD est présentée sur la Figure 3.2, basée sur l' Équation 3.2. Au début de l'EPD, la concentration des QD est constante dans la solution qui infiltre le film mésoporeux.

L'application du champ électrique externe induit l'accroche des QD sur le TiO<sub>2</sub>. Ce processus cause une baisse de la concentration des QD dans la solution infusée dans la couche de TiO<sub>2</sub> mésoporeux, alors que la concentration en QD à l'extérieur du film de TiO<sub>2</sub> reste constante. Le gradient de concentration créé à la surface, dû à la déplétion de la solution dans le TiO<sub>2</sub> est bien visible, tout comme l'est l'évolution de la concentration en PbS en fonction de la profondeur menant à la concentration finale après une longue durée d'EPD.

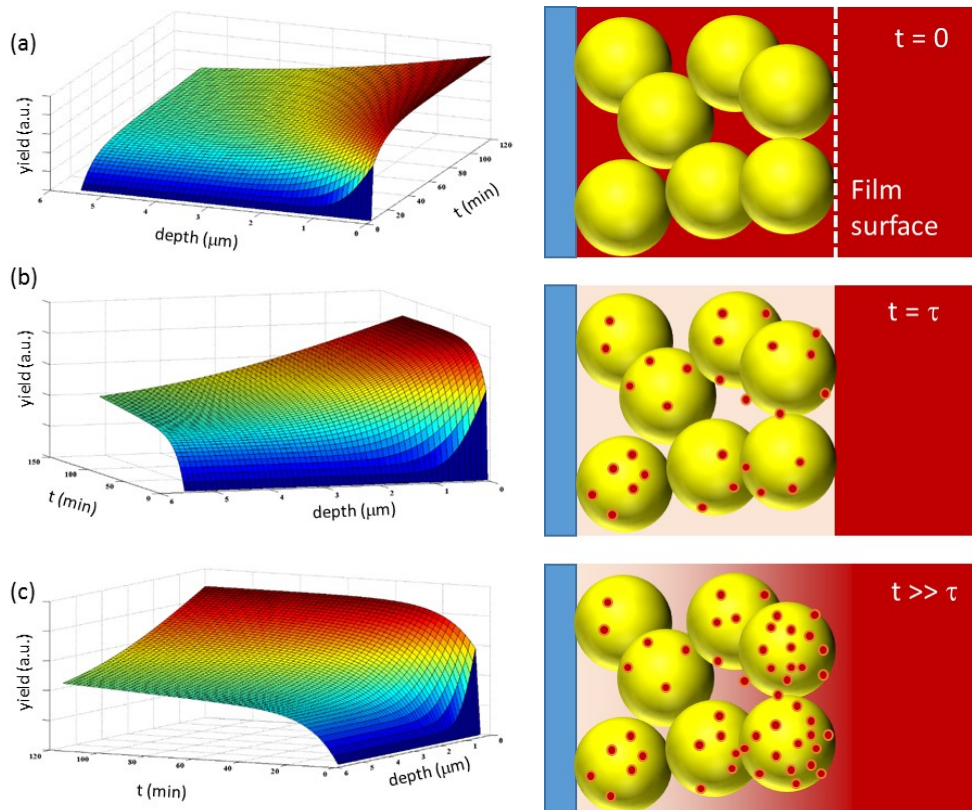


**Figure 3.2** Distribution en Pb en fonction du temps et de la profondeur dans le film de TiO<sub>2</sub> vu sous trois perspectives différentes, basé sur les paramètres expérimentaux calculés pour une tension de 200V.

De plus, nous avons étendu l'étude de L'EPD pour différents voltages. L'application de 50 V n'induit qu'une diffusion négligeable, et la quantité de QD est due est quasiment due à l'absorption native de la solution. Dès que le voltage appliqué augmente, la fraction du Pb venant de la diffusion augmente. A 200 V, après 120 minutes, plus de 40% du Pb absorbé par le TiO<sub>2</sub> vient de la diffusion de la solution

externe, ce qui nous indique que ce processus ne peut être négligé lors de la préparation de ces systèmes composites.

#### 4. PERSPECTIVES

Pour résumer, nous avons investigué l'absorption de QD NIR Cœur@coquille produit de manière *ex-situ* dans des films mésoporeux de TiO<sub>2</sub> par EPD. Nous avons démontré une couverture homogène et sans agrégation entre eux des QD, et une stabilité améliorée des QD cœur@coquille par rapport à l'oxydation et la formation de défaut après EPD, comparé au QD en PbS pur. Nous avons étudié la dynamique de l'absorption par EPD par RBS. Le procédé complet peut être analysé comme suit : premièrement, la concentration en QD est constante dans la solution infusée dans le film mésoporeux, et le champ électrique induit l'attachement des QD sur la surface du TiO<sub>2</sub>. Puis, la déplétion des QD en solution génère un gradient de QD ce qui induit par une diffusion de type loi de Fick. Le coefficient de diffusion D montre une augmentation du champ électrique, ce qui n'est pas encore explicable en l'état et nécessite des études complémentaires.

Ces résultats démontrent sans aucun doute que l'absorption des QD peut être contrôlée finement par le contrôle fin des paramètres d'EPD, et nous donne une description rationnelle et quantitative des méthodes de fabrication des photoanodes catalysées optiquement pour QDSC. Ces résultats peuvent être mis à profit afin d'optimiser les processus de catalyse optique par des QD de films mésoporeux pour des QDSC et peuvent être appliqués, en principe, à d'autres types de nanocristaux semi-conducteurs usuellement utilisés pour la catalyse optique des électrodes mésoporeuses.

## RÉFÉRENCES

- [1] U. Cubasch, G. A. Meehl. In Climate Change 2001: The Scientific Basis. *Ed. J. T. Houghton, Cambridge Univ. Press*, Cambridge, 2001, 525–582.
- [2] D. Wilson. We Have the Power; Inside Story. *The Sun Herald*, 2006, 8.
- [3] K. Tvrdy, P. A. Frantsuzov, and P. V. Kamat. Photoinduced Electron Transfer from Semiconductor Quantum Dots to Metal Oxide Nanoparticles. *Proc. Natl. Acad. Sci. U. S. A.*, 2011, 108, 29-34.
- [4] P. V. Kamat, K. Tvrdy, D. R. Baker, and J. G. Radich. Beyond Photovoltaics: Semiconductor Nanoarchitechtures for Liquid Junction Solar Cells. *Chem. Rev.*, 2010, 110, 6664-6688.
- [5] D. M. Chapin, C. S. Fuller, and G. L. Pearson. A New Silicon p-n Junction Photocell for Converting Solar Radiation into Electrical Power. *Journal of Applied Physics*, 1954, 25 (5), 676–677.
- [6] A. L. Rogach, L. Katsikas, A. Kornowski, D. Su, A. Eychmüller, H. Weller, Ber. Bunsen. Synthesis and characterization of thiol-stabilized CdTe nanocrystals. *Phys. Chem.*, 1996, 100, 1772 – 1778.
- [7] L. E. Brus. Electron-electron and Electron-hole Interactions in Small Semiconductor Crystallites-the Size Dependence of the Lowest Excited Electronic State. *Journal of Chemical Physics*, 1984, 80, 4403–4409.
- [8] A. Zaban, O. I. Micic, B. A. Gregg, A. J. Nozik. Photosensitization of Nanoporous TiO<sub>2</sub> Electrodes with InP Quantum Dots. *Langmuir*, 1998, 14, 3153–3156.
- [9] A. J. Nozik. Quantum Dot Solar Cells. *Phys. E*, 2002, 14, 115–120.
- [10] P. V. Kamat,. Quantum Dot Solar Cells. Semiconductor Nanocrystals as Light Harvesters. *J. Phys. Chem. C*, 2008, 112, 18737–18753.

- [11] H. Lee, H. C. Leventis, S. J. Moon, P. Chen, S. Ito, S. A. Haque, T. Torres, F. Nuesch, T. Geiger, S. M. Zakeeruddin et al. PbS and US Quantum Dot-Sensitized Solid-State Solar Cells: Old Concepts, New Results. *Adv. Funct. Mater.*, 2009, 19, 2735–2742.
- [12] J. M. Luther, M. Law, M. C. Beard, Q. Song, M. O. Reese, R. J. Ellingson, A. J. Nozik. Schottky Solar Cells Based on Colloidal Nanocrystal Films. *Nano Lett.*, 2008, 8, 3488–3492.
- [13] R. Debnath, J. Tang, D. A. Barkhouse, X. Wang, A. G. Pattantyus-Abraham, L. Brzozowski, L. Levina, E. H. Sargent. Ambient-Processed Colloidal Quantum Dot Solar Cells via Individual Pre-Encapsulation of Nanoparticles. *J. Am. Chem. Soc.*, 2010, 132, 5952–5953.
- [14] <http://www.sigmaaldrich.com/materials-science/nanomaterials/quantum-dots.html>.
- [15] [http://commons.wikimedia.org/wiki/File:Solar\\_Spectrum.png](http://commons.wikimedia.org/wiki/File:Solar_Spectrum.png).
- [16] A. Braga, S. Giménez, I. Concinia, A. Vomiero, and I. Mora-Seró. Panchromatic Sensitized Solar Cells Based on Metal Sulfide Quantum Dots Grown Directly on Nanostructured TiO<sub>2</sub> Electrodes. *J. Phys. Chem. Lett.*, 2011, 2 (5), 454–460.
- [17] Y. L. Lee, B. M. Huang, H. T. Chien. Highly Efficient CdSe-Sensitized TiO<sub>2</sub> Photoelectrode for Quantum-Dot-Sensitized Solar Cell Applications. *Chem. Mater.*, 2008, 20, 6903–6905.
- [18] O. Niitsoo, S. K. Sarkar, C. Pejoux, S. Ruhle, D. Cahen, G. Hodes. Chemical Bath Deposited CdS/CdSe-Sensitized Porous TiO<sub>2</sub> Solar Cells. *J. Photochem. Photobiol. A*, 2006, 181, 306–313.
- [19] A. G. Pattantyus-Abraham, I. J. Kramer, A. R. Barkhouse, X. Wang, G. Konstantatos, R. Debnath, L. Levina, I. Raabe, M. K. Nazeeruddin, M. Gratzel, E. H. Sargent. Depleted-Heterojunction Colloidal Quantum Dot Solar Cells. *ACS Nano*, 2010, 4, 3374–3380.

- [20] P. Sarkar, P. S. Nicholson. Electrophoretic Deposition (EPD): Mechanisms, Kinetics, and Application to Ceramics. *J. Am. Ceram. Soc.*, 1996, 79, 1987–2002.
- [21] A. R. Boccaccini, J. A. Roether, B. J. C. Thomas, M. S. P. Shaffer, E. Chavez, E. Stoll, E. J. Minay. The electrophoretic deposition of inorganic nanoscaled materials : A review. *J. Ceram. Soc. Jpn.*, 2006, 114 (1), 1–14.
- [22] M. E. Wong, P. C. Searson. ZnO Quantum Particle ThinFilms Fabricated by Electrophoretic Deposition. *Appl. Phys.Lett.*, 1999, 74, 2939–2941.
- [23] S. V. Mahajan, J. Cho, M. S. P. Shaffer, A. R. Boccaccini, J. H. Dickerson. Electrophoretic Deposition and Characterization of Eu<sub>2</sub>O<sub>3</sub> Nanocrystal\_Carbon Nanotube Heterostructures. *J. Eur. Ceram. Soc.*, 2010, 30, 1145–1150.
- [24] M. Giersig, P. Mulvaney. Formation of Ordered Two-Dimensional Gold Colloid Lattices by Electrophoretic Deposition. *J. Phys. Chem.*, 1993, 97, 6334–6336.
- [25] M. N. Patel, R. D. Williams, R. A. May, H. Uchida, K. J. Stevenson, K. P. Johnston. Electrophoretic Deposition of Au Nanocrystals inside Perpendicular Mesochannels of TiO<sub>2</sub>. *Chem. Mater.*, 2008, 20, 6029–6040.
- [26] L. Grinis, S. Dor, A. Ofir, A. Zaban. Electrophoretic Deposition and Compression of Titania Nanoparticle Films for Dye-Sensitized Solar Cells. *J. Photochem. Photobiol. A*, 2008, 198, 52–59.
- [27] B. Ferrari, A. Bartret, C. Baudin. Sandwich Materials Formed by Thick Alumina Tapes and Thin-Layered Alumina\_Aluminium Titanate Structures Shaped by EPD.J. *Eur. Ceram. Soc.*, 2009, 29, 1083–1092.
- [28] M. Vidotti, S. I. C. de Torresi. Electrostatic Layer-by-Layer and Electrophoretic Depositions as Methods for Electrochromic Nanoparticle Immobilization. *Electrochim. Acta*, 2009, 54, 2800–2804.

- [29] N. J. Smith, K. J. Emmett and S. J. Rosenthal. Photovoltaic cells fabricated by electrophoretic deposition of CdSe nanocrystals. *Appl. Phys. Lett.*, 2008, 93, 043504.
- [30] A. Salant, M. Shalom, I. Hod, A. Faust, A. Zaban, U. Banin. Quantum Dot Sensitized Solar Cells with Improved Efficiency Prepared Using Electrophoretic Deposition. *ACS Nano*, 2010, 4, 5962–5968.
- [31] N. P. Benehkohal, V. González-Pedro, P. P. Boix, S. Chavhan, R. Tena-Zaera, G. P. Demopoulos, and I. Mora-Seró. Colloidal PbS and PbSeS Quantum Dot Sensitized Solar Cells Prepared by Electrophoretic Deposition. *J. Phys. Chem. C*, 2012, 116 (31), 16391–16397.
- [32] I. Hod, V. González-Pedro, Z. Tachan, F. Fabregat-Santiago, I. Mora-Seró, J. Bisquert, and A. Zaban. Dye versus Quantum Dots in Sensitized Solar Cells: Participation of Quantum Dot Absorber in the Recombination Process. *J. Phys. Chem. Lett.*, 2011, 2 (24), 3032–3035.
- [33] K. Szendrei, M. Speirs, W. Gomulya, D. Jarzab, M. Manca, O. V. Mikhnenko, M. Yarema, B. J. Kooi, W. Heiss and M. A. Loi. Exploring the Origin of the Temperature-Dependent Behavior of PbS Nanocrystal Thin Films and Solar Cells. *Adv. Funct. Mater.*, 2012, 22, 1598–1605.
- [34] J. Tang, K. W. Kemp, S. Hoogland, K. S. Jeong, H. Liu, L. Levina, M. Furukawa, X. H. Wang, R. Debnath, D. K. Cha, K. W. Chou, A. Fischer, A. Amassian, J. B. Asbury, E. H. Sargent. Colloidal-quantum-dot photovoltaics using atomic-ligand passivation. *Nature Materials*, 2011, 10 (10), 765-771.
- [35] B. O. Dabbousi, J. RodriguezViejo, F. V. Mikulec, J. R. Heine, H. Mattoussi, R. Ober, K. F. Jensen, M. G. Bawendi. (CdSe) ZnS core-shell quantum dots: Synthesis and characterization of a size series of highly luminescent nanocrystallites. *Journal of Physical Chemistry B*, 1997, 101 (46), 9463-9475.

- [36] L. Dworak, V. V. Matylitsky, V. V. Breus, M. Braun, T. Basche, J. Wachtveitl. Ultrafast Charge Separation at the CdSe/CdS Core/Shell Quantum Dot/Methylviologen Interface: Implications for Nanocrystal Solar Cells. *Journal of Physical Chemistry C*, 2011, 115 (10), 3949-3955.
- [37] H. Zhao, T. Zhang, M. Chaker, and D. Ma. Ligand and Precursor Effects on the Synthesis and Optical Properties of PbS Quantum Dots. *Journal of Nanoscience and Nanotechnology*, 2010, 10, 4897–4905.
- [38] J. M. Pietryga, D. J. Werder, D. J. Williams, J. L. Casson, R. D. Schaller, V. I. Klimov, and J. A. Hollingsworth. Utilizing the Lability of Lead Selenide to Produce Heterostructured Nanocrystals with Bright, Stable Infrared Emission. *Journal of the American Chemical Society*, 2008, 130, 4879–4885.
- [39] H. Zhao, M. Chaker, and D. Ma. Effect of CdS Shell Thickness on the Optical Properties of Water-soluble Amphiphilic Polymer Encapsulated PbS/CdS Quantum Dots. *Journal of Materials Chemistry, J. Mater. Chem.*, 2011, 21, 17483-17491.
- [40] H. G. Zhao, M. Chaker, N. Q. Wu, D. L. Ma. Towards controlled synthesis and better understanding of highly luminescent PbS/CdS core/shell quantum dots. *Journal of Materials Chemistry*, 2011, 21 (24), 8898-8904.
- [41] H. Zhao , Z. Fan , H. Liang , G. S. Selopal , B. A. Gonfa , L. Jin , A. Soudi , D. Cui , F. Enrichi , M. M. Natile , I. Concina , D. Ma , A. O. Govorov , F. Rosei and A. Vomiero. Controlling photoinduced electron transfer from PbS@CdS core@shell quantum dots to metal oxide nanostructured thin films. *Nanoscale*, 2014, 6, 7004-7011.
- [42] Kevin Tvrdy. Electron transfer reaction in quantum dot sensitized solar cells. *University of Notre Dame*, 2011, 16-17.

- [43] T. Zhang, H. G. Zhao, D. Riabinina, M. Chaker, D. L. Ma. Concentration-Dependent Photoinduced Photoluminescence Enhancement in Colloidal PbS Quantum Dot Solution. *Journal of Physical Chemistry C*, 2010, 114 (22), 10153-10159.
- [44] H. G. Zhao, D. F. Wang, T. Zhang, M. Chaker, D. L. Ma. Two-step synthesis of high-quality water-soluble near-infrared emitting quantum dots via amphiphilic polymers. *Chemical Communications*, 2010, 46 (29), 5301-5303.
- [45] M. A. Islam, Y. Q. Xia, D. A. Telesca, M. L. Steigerwald, I. P. Herman. Controlled Electrophoretic Deposition of Smooth and Robust Films of CdSe Nanocrystals. *Chem.Mater.*, 2004, 16, 49–54.
- [46] R. Krishnan, M. A. Hahn, Z. Yu, J. Silcox, P. M. Fauchet, T. D. Krauss. Polarization Surface-Charge Density of Single Semiconductor Quantum Rods. *Phys. Rev. Lett.*, 2004, 92 (21), 216803(1) - 216803(4).
- [47] G. Kalyuzhny, R. W. Murray. Ligand Effects on Optical Properties of CdSe Nanocrystals. *J. Phys. Chem. B*, 2005, 109, 7012-7021.